


Understanding Posterior Staphyloma in Pathologic Myopia: Current Overview, New Input, and Perspectives

Adèle Ehongo 

Ophthalmology Department, Erasmus Hospital, Brussels, Belgium

Correspondence: Adèle Ehongo, Ophthalmology Department, Erasmus Hospital, Route de Lennik 808, Brussels, 1070, Belgium, Tel +3225553114, Fax +3225556737, Email adele.ehongo@erasme.ulb.ac.be

Abstract: Posterior staphyloma (PS) is considered the hallmark of pathologic myopia and is defined as an outpouching of a circumscribed portion of the eyeball with a radius of curvature smaller than that of the adjacent zone. Although more common in eyes with high myopia, it can affect those without it. The presence of PS is associated with a structurally and functionally worse course of high myopia that can lead to visual disability. Unfortunately, the pathogenesis of PS is unclear so far. Thus, due to the increasing prevalence of myopia which has been further exacerbated by the advent of COVID-19 lockdown, researchers are eager to elucidate the pathogenesis of pathologic myopia and that of its complications, especially PS, which will allow the development of preventive strategies. The aim of this work was to review the morphological characteristics of PS with emphasis on similarities with peripapillary staphyloma and to discuss the pathogenesis of PS considering recent suggestions about that of peripapillary staphyloma.

Keywords: myopia, staphyloma, pathogenesis, optical coherence tomography, oblique muscles, optic nerve sheaths

Introduction

Myopia is one of the major contributors to moderate and severe visual impairment worldwide.¹ Before the COVID-19 era, projections for 2050 announced 50% of people worldwide with myopia and 10% with high myopia (HM),² leading to an increase in myopia-related complications.³ The prevalence of myopia may even be higher than expected, as the COVID-19 pandemic has led to an increase in children's screen time and indoor activities, with a decrease in their outdoor activities. Confirming these fears, early studies comparing myopia status in children before and during the COVID-19 lockdown found a significant myopic shift,⁴ a significantly higher rate of myopia progression,⁴⁻⁷ as well as a significantly higher prevalence⁶ of eyes showing progression of myopia during the pandemic. Increased digital screen time was particularly associated with a greater myopia progression.⁸ Therefore, without effective joint forces, this increase in refractive development could be dramatically followed by myopic complications in the decades to come.

Beyond the poor quality of life of those affected, the burden of myopia-related visual impairment amounts to billions of US dollars, making myopia a major public health issue, and mobilizing efforts to understand the mechanisms that lead to it and promote its complications.³

The term pathologic myopia (PM) refers to ocular complications of myopia, characterized by typical degenerative changes in the sclera, choroid and retina that can lead to visual impairment.⁹ HM is just a higher degree of myopia defined by a spherical equivalent refractive error of - 6.00 or greater,⁹ or an axial length (AL) ≥ 26.5 mm. Furthermore, although PM primarily affects eyes with HM, it can occur in non-highly myopic eyes.^{10,11} PM encompasses myopic maculopathy, myopic-associated neuropathy, and posterior staphyloma (PS) with its complications.

Although the pathogenesis of PS is currently unclear, it has recently been suggested that peripapillary staphyloma (PPS), classified as PS type III,¹² is promoted by the pulling force of the optic nerve (ON) sheaths on their scleral insertions.¹³ It has even been shown that the amplitude of the forces deployed by these sheaths reaches that of the extraocular muscles.¹⁴ The

concept of deformation of the eyeball by traction or compression exerted by structures inserting on its surface is attractive and may constitute an advance in understanding the pathogenesis of other types of PS.

The objective of this work was first, to make an overview of PS. Then, based on the similarities between the morphological characteristics of PPS and those of other PS, discuss the pathogenesis of PS. Potential perspectives for understanding the pathophysiology of PS are finally suggested.

Background, Definition, Prevalence

PS was first described by Antonio Scarpa¹⁵ in 1801 from a pair of postmortem eyes. Based on ophthalmoscopic appearance and with the aid of drawings, Curtin¹² classified PS into ten types: five primaries (I to V) and five compounds (VI to X). PS was unequivocally defined by Spaide¹⁶ as an outpouching of a circumscribed portion of the eye wall with a radius of curvature shorter than that of the adjacent wall. However, a sharp outpouching of the wall of the eye is not always found in all the cases of PS.¹⁷

Analyzing the overall shape of the eye using three-dimensional magnetic resonance imaging (3D-MRI) was a major turning point.¹⁰ 3D-MRI allowed the full capture of large PS,^{10,17,18} and was subsequently used to refine the diagnostic criteria for PS using other methods.^{17–20}

First, of the ten initial types of PS,¹² six revised types have been proposed,¹⁷ based on a combination of 3D-MRI and ultra-widefield (UWF) fundus photos, in addition to the relative location of PS to papilla, macula, and according to the size: wide macular (Type I), narrow macular (Type II), nasal (Type IV), inferior (Type V), others (Type VI) and PPS.¹⁷

As 3D-MRI is not suitable for conventional clinical conditions, Ohno-Matsui et al also conducted a point-to-point correlation analysis between the whole shape of the eye on 3D-MRI and its appearance on UWF fundus photos to make the classification useful for clinicians.¹⁷

Then, as despite the use of 3D-MRI, some PS (PPS and type IV) presented only as a nasal distortion of the globe,¹⁷ with rather subtle and narrow changes in their curvature, making them difficult to diagnose, the next improvement was SS-OCT.^{18,19} It showed higher resolution, detecting small and discrete cases of PS and revealing changes in the choroid and sclera at the edge of a PS.^{18,19}

Finally, the size of some PS being very wide or the depth too steep to fit in the length or width of a scan, their diagnosis benefited from additional improvement that overcame these flaws: the Widefield SS-OCT (WF-OCT).^{18,20} Therefore, the diagnosis of PS is currently considered best made using WF-OCT.^{18–20}

The latest novelty is a prototype of a WF-OCT that uses multiple scan lines, generating scan maps that allow 3D reconstruction of PS in a region of interest.^{18,20} It provides high-resolution 3D images of PS and measurements of their size and volume.^{18,20}

The prevalence of PS in highly myopic eyes is between 10.9% and 92.8%.^{21,22} This discrepancy results from different diagnostic methods,^{12,17,21–27} definitions,^{16,23} origins of populations,^{21,22,28} ages,^{12,21} and whether they were hospital-based,^{22–25,27} or population-based studies.^{17,21,28} Even recently, with the use of 3D-MRI, two studies showed a difference in prevalence, which could result from the specificities of these reference centers.^{17,29}

PS is mostly bilateral^{22,25} and both eyes of bilateral cases have essentially the same ocular shape^{10,12}, and PS subtype.^{10,22,25,29} Moreno et al found that bilateral cases had longer AL and more severe PM than unilateral cases.²² In unilateral cases, the AL-difference between the two eyes of the subjects was larger.²²

Types I and II were the most predominant, accounting for 55–74% and 8–26.7% of PS eyes respectively.^{12,25} PPS, has also suffered from the lack of diagnostic accuracy and has been considered as relatively rare. However, its prevalence found by Curtin (7 eyes, 1.5%)¹² and Ohno-Matsui et al (5 eyes, 2.5%)¹⁷ is lower than in recent series: 4.3%–6.9%.^{23,25,28} Using multimodal imaging, including UWF fundus photos, PPS was even the most common subtype in Moreno et al series (62 eyes, 20%).²²

Diagnosis

As just discussed, efforts to diagnose PS have been longstanding. Stereoscopic fundus examination^{12,19,20,22} is subjective. The full extent of some PS is missed in conventional 45° or 50° fundus photos,^{21,23} resulting in their underdiagnosis.¹⁸ Many conventional OCT fail to capture the full extent of wide PS.^{1,21,30} B-scan ultrasound,^{23,24,26,31} provides only 2D approach which difficultly enables to reconstruct large PS.¹⁸ Ultimately, tomodesitometry^{32,33} and MRI,³⁴ which were sometimes used are not suitable for diagnosing PS. Table 1 summarizes the methods of diagnosing PS.

Table I Methods for Diagnosing Posterior Staphyloma

Representative References	Methods	Advantages	Major Advance	Drawbacks/Shortcomings/Flaws
1977 Curtin ¹²	Indirect ophthalmoscopy.	Stereoscopic view of the fundus.	Criteria to diagnose the 10 types of PS.	Subjective.
1984 Swayne ³³	Computed tomography.	Quantitative measurements are affordable. It enables axial, vertical, and horizontal comparisons.	/	2D only, the complete topography of the PS not provided. Not suitable for PS diagnosis in routine.
2008 Hsiang ²³	B-mode Ultrasound.	More reliable and objective than simple observation. Possibility of quantification.	/	Only a 2D approach. Not easy to reconstruct 3D shape of large PS.
2011 Gao ²⁸	Fundus photos: 45° or 50°.	More reliable and objective than simple ophthalmoscopy.	/	2D only. Large PS edges not detected. Some PS underdiagnosed. No information on depth.
2011 Malhortra ³⁴	Magnetic resonance Imaging (MRI).	Quantitative measurements are affordable. Enables axial, vertical, and horizontal comparisons.	/	Time-consuming, financial barriers, contraindicated in patients with metals. No information on retina and choroid due to low resolution (1) Not accurate in clinical settings.
2011 Moriyama ¹⁰	3D-MRI.	First imaging of the entire eye. Reliable quantitative measurements.	Establishes the 4 shapes of pathologic myopic eyes using 3D-MRI.	3D-MRI not available in many clinical settings. Slight changes in curvature not detected by 3D-MRI. In addition to (1).
2012 Ohno-Matsui ³⁵	SS-OCT (+3D-MRI)	Enables visualization of retina, choroid and inner scleral contour in the same scan. Enables to establish the relationship between fundus lesions and OCT aspects of retina, choroid and sclera.	Correlation between the slope of the posterior sclera on OCT and eye shape on 3D-MRI.	The posterior scleral contour not seen in all the eyes with SS-OCT.
2013 Henaine-Berra ³⁰	SD-OCT.	Enables visualization of retina and choroid in addition to the anterior scleral curvature.	/	Conventional OCT imaging is limited in depth and extent.
2014 Ohno-Matsui ¹⁷	Combination of 3D-MRI and ultra-widefield fundus photos.	Allows detection of large PS underdiagnosed using 45–50° fundus photos. The edges of PS present pigmentary abnormalities and are helpful landmarks to diagnose it.	Criteria to diagnose the 6 types of PS.	Subtle PS still difficult to detect with 3D-MRI.
2014 Ohno-Matsui ¹⁷	Ultra-widefield fundus photos.	The edges of PS are characterized by the presence of pigment abnormalities on color photos, abnormal autofluorescence, and abnormal reflectance in infrared imaging, using ultra-widefield fundus photos such as OptosT [®] .	Criteria to diagnose PS using ultra ultra-widefield fundus photos.	2D only. No information on depth.

(Continued)

Table I (Continued).

Representative References	Methods	Advantages	Major Advance	Drawbacks/Shortcomings/Flaws
2017 Shinohara ²⁰	Widefield OCT and its 3D rendering aptness.	OCT definition of PS. 3 key features: a gradual choroidal thinning toward the PS edge, an inward protrusion of the sclera at PS edges, an outward protrusion of sclera in the area posterior to the PS edges. Best tool recommended for the diagnosis of PS. Achieves previously unattainable 3D resolution for diagnosing PS using OCT.	Criteria to diagnose PS using widefield OCT.	Wide-field OCT is not widely available in routine.
2019 Tanaka ³⁶	Ultra-widefield OCT.	In the early stage, the inward scleral deformation at the edge of a PS may be absent. Therefore, PS shows a gradual thinning of the choroid toward the PS edge, a gradual re-thickening of choroid from the PS edge toward the posterior pole and the outward scleral deformation.	Criteria to detect subtle PS margins using widefield OCT.	Wide-field OCT is not widely available in routine.

Abbreviations: PS, Posterior staphyloma; 2D, Two-dimensional; 3D, Three-dimensional; MRI, Magnetic resonance Imaging; OCT, optical coherence tomography; WF-OCT, widefield optical coherence tomography; 3D-MRI, Three-dimensional magnetic resonance imaging; SD-OCT, spectral domain optical coherence tomography; SS-OCT, swept source optical coherence tomography.

Diagnosing Posterior Staphyloma Using UWF Photos

A comparison between 3D-MRI and UWF photos allowed to obtain the following diagnostic criteria at the border of the PS:¹⁷ pigment anomalies (Figure 1), hypo-auto-fluorescent lines on auto-fluorescent filter and hypo or hyperreflectant lines on infrared light.¹⁷

Diagnosing PPS

Shinohara et al¹⁹ combined stereoscopic fundus examination and SS-OCT to characterize PPS.



Figure 1 Fundus image of a posterior staphyloma (PS). Highly myopic eye with a PS type I according to Curtin's classification. The borders of the PS show pigment anomalies.

On stereoscopic fundus, the PPS showed “a slight excavation around the optic disc”. The edge of this excavation presented pigmentary abnormalities,^{17,19} it was distinct from, and extended beyond the margin of the peripapillary conus.¹⁹ (Figure 2A).

In OCT, PPS was defined as a gently sloping excavation clearly observed around the optic disc and seen at least half around it.¹⁹ Additionally, the sclera showed a posterior bowing with the local curvature steeper than the adjacent scleral regions and an inward elevation at the edge of the PPS. The choroid showed thinning at the edge of the PPS¹⁹ (Figure 2B). It should be noted that all the figures provided by these authors show that the thinning of the choroid was followed by re-thickening in front of the posterior bowing of the sclera (Figure 2B).

Diagnosing Wide Staphyloma Using OCT

On WF-OCT, a PS consistently shows 3 features: a gradual choroidal thinning toward the PS edge, an inward protrusion of the sclera at the PS edge, an outward protrusion of sclera in the area posterior to the edges of PS.^{18,20} (Figure 3).

Subsequently, Tanaka et al showed that the inward protrusion of the sclera at the edge of a PS is not always obvious in younger subjects.³⁶ Nonetheless, the choroid exhibits thinning towards the edge of PS, followed by re-thickening along the outward protrusion of the sclera.³⁶

PS diagnosis is best accomplished using widefield imaging^{17,18,20} (Figure 4A–C).

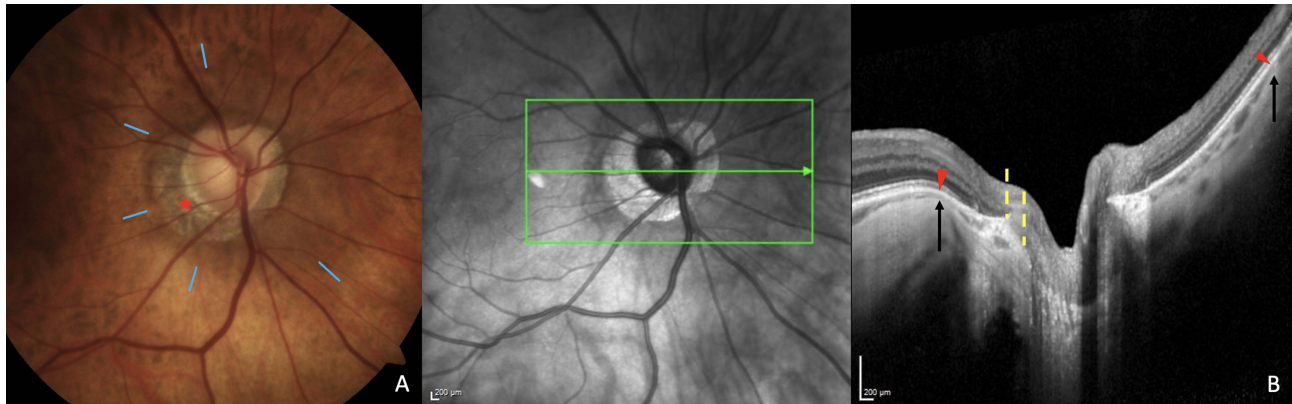


Figure 2 Characteristics of a peripapillary staphyloma (PPS). (A) Fundus image. The PPS presents slight pigmentary changes at its border (blue lines). Its temporal border extends beyond the margin of the conus (red star). (B) The OCT section is along the arrow in the infrared image. The sclera shows a posterior bowing with the local curvature steeper than the adjacent scleral regions between the black arrows. The sclera also shows an inward elevation (black arrows) at the border of the PPS, while the choroid presents a thinning at this edge (between red arrowhead and black arrow) followed by a rethickening toward the optic nerve. The myopic conus is between the dashed yellow lines.

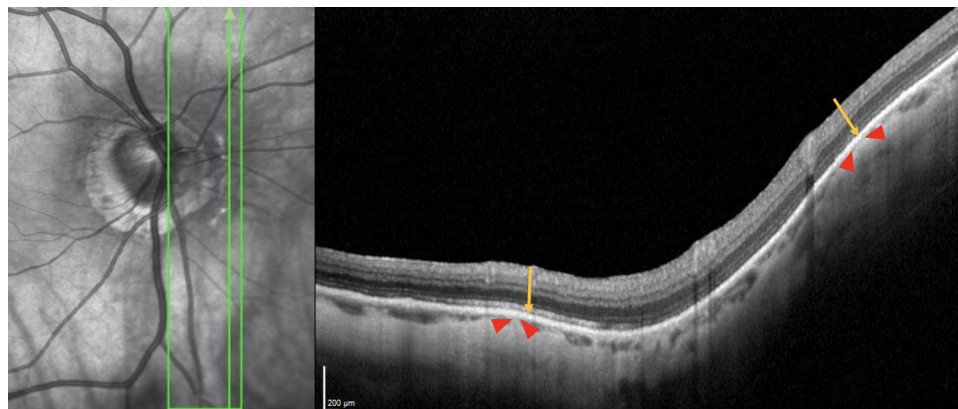


Figure 3 OCT features of a posterior staphyloma (PS). The section is along the arrow in the infrared image. The PS shows a gradual thinning of the choroid from the periphery toward the PS edge (red arrowheads) and a gradual re-thickening of the choroid from the PS edge in direction to the posterior pole, accompanied by a change in the curvature radius (yellow arrows) of the sclera at the PS edge.

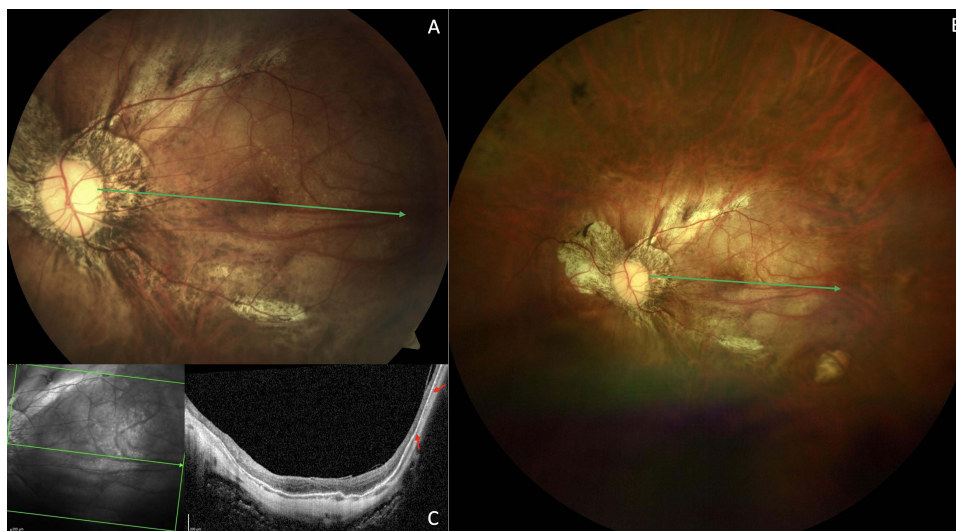


Figure 4 Illustration of type I posterior staphyloma (PS) revealing the advantage of wide-field imaging. **(A)** In 50° imaging with Visucam®, the PS is not obvious. **(A–C)** The green arrows indicate the location of OCT section in **(C)**. **(B)** In 240° imaging with Clarus®, Type I PS is clearly obvious. **(C)** OCT section captured by the posterior pole module of the Glaucoma premium edition of Spectralis®. The temporal edge of this PS is outlined by red arrows and is just at the limit of the acquisition width, while its nasal edge is not captured.

Risks Factors

Age

The prevalence of PS increases with age^{17,21,35,37} and subjects with PS are significantly older than those without.^{17,21,23,25,27,29,38} Moreno et al showed that the risk of PS increased by 10% per year of age.³⁸ Even in eyes without long AL, Wang et al, pointed out that those with PS belonged to older subjects.¹¹

Analyzing the prevalence of each type of PS by age group, Curtin showed a decrease in type I and II while that of other subtypes increased with age.¹² Shinohara et al found that subjects with both HM and PPS were younger than those without HM.²⁰ This means that PPS occurs earlier in eyes with HM, than in those without HM, which is consistent with ON sheaths traction being stronger in eyes with HM^{39–41} or eyes with HM being more sensitive to this traction. Additionally, this suggests that ON sheaths traction needs more time to promote PPS in eyes without HM.

Finally, Ohno-Matsui et al found that in eyes with HM, those with irregular curvature had PS and belonged to older subjects.³⁵

Thus, with increasing age, PS increases in prevalence and in severity as it will be discussed in section “quantitative aspects and long-term changes”.

Axial Length

No statistically significant difference in AL was found between eyes with and without PS in previous series,^{12,17,21} but recent studies have reported that longer AL was significantly more common in eyes with than without PS^{26,27} and that the prevalence of PS increased with the increasing AL.³⁷ Moreover, Moreno et al found that the risk of PS increased by 132% per each millimeter of growth of AL.³⁸

The presence of PS in eyes with short AL^{10,11,20} and in non-highly myopic eyes^{10,20} suggests that the lengthening of the eye would not be the factor triggering the appearance of PS. However, as HM has been shown to lead to thinning and weakening of the tissues,^{42–45} these changes instead increase the sensitivity of myopic eyes to factors promoting PS and explain the higher frequency of PS in HM. Finally, as AL measurement is fovea-based it may be shorter than the maximum length of the eye in types III, IV and V PS.^{16,18–20} This may explain why AL is significantly longer in eyes with wide macular PS²⁵ and in compound PS.²⁵

On the other hand, eyes with irregular scleral curvature were found to have significantly longer AL than those with other curvatures,^{21,24,35} supporting the hypothesis that the stretched and extremely thin sclera fails to maintain its normal

curvature.²¹ Very recently, the depth-to-diameter ratio of type II PS was shown to correlate with AL,⁴⁶ implying that the severity of some PS is related to AL.

Gender

Numa et al studied the prevalence of PS in the Japanese population and found no significant difference between males and females, consistent with previous reports.²¹ Interestingly, they showed that the shape of the PS was steeper and less smooth in females.²¹ Therefore, they suggested that women with HM were likely to visit the hospital more frequently than men, which would explain why many studies looking at the complications of HM have included more women.^{10,21,22,25,27,28,46,47} The reason of why the curvature of the eye is less smooth in women remains to be clarified.

In contrast, 2 population-based studies have found a significantly higher prevalence of PS in women,^{1,31} which deserves confirmation.

Histomorphometry, Ultrastructure, Microvasculature

In PS, all ocular layers have been studied and show modifications which can be divided into myopia-related degenerations and specific features at the edge and within the PS. High-resolution OCT has greatly facilitated in vivo assessment of these changes.

Nonspecific Myopic Changes

Scleral thinning in HM is largely confined to the posterior pole of the eye.^{1,35,48–50} Rather than simple passive stretching and tissue redistribution, this thinning results from tissue loss^{43,48} involving a decrease in collagen production, and an increase in collagen degradation.⁴⁸ A change in glycosaminoglycans content^{50–52} may also be involved. Electron microscopy reveals changes in collagen fiber bundle arrangement⁴² and an accumulation of small diameter fibrils.^{42,48}

In addition to structural thinning of the choroid,^{1,35,53,54} a significant reduction in choroidal blood flow⁵⁴ and choroidal vascular index related to axial elongation⁵³ has been documented. An active mechanism is also suggested in choroidal thinning.⁵⁴

Specificities of Posterior Staphyloma

On histology, myopic PS were characterized in their center by marked scleral thinning and pronounced de-arrangement of scleral collagen fibrils.^{31,50} Scleral thinning started abruptly at the edge of the PS.⁵⁰

OCT changes in reflectivity demonstrates this scleral remodeling (Figure 5). Some breaks on BM⁵⁰ are also evident (Figure 5). Ohno-Matsui et al found that all the eyes with irregular curvature had thinner subfoveal scleral thickness than any other type.³⁵ This scleral thinning was also disclosed by Zhou et al by comparing myopic eyes with and without PS.¹

A key determining factor of PS is thinning of the choroid at its edge.^{19,20} It adds to the choroidal thinning associated with axial elongation.^{18–20} (Figure 5). Moreover, the subfoveal choroid has been shown to be significantly thinner in eyes with than

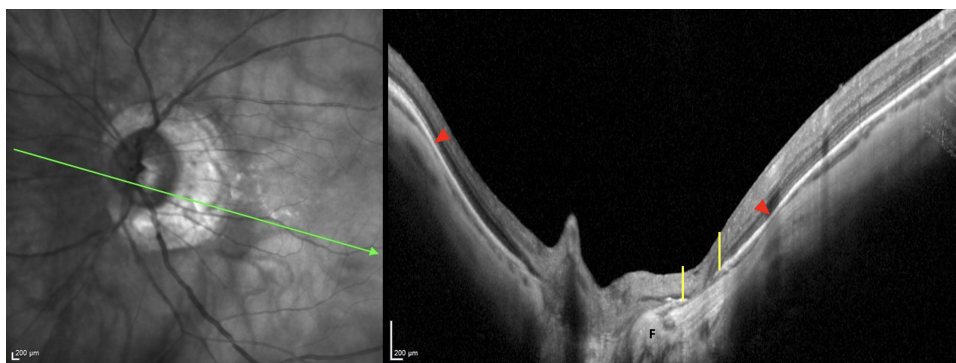


Figure 5 Scleral changes and peripapillary staphyloma (PPS). OCT section along the arrow in the infrared image. Gradual thinning of the choroid at the edge of the PPS (red arrowheads), followed by a gradual re-thickening of the choroid towards the posterior pole. The sclera shows changes in reflectivity at the level of the scleral flange (F), suggesting remodeling of its structure. In addition, a Bruch's membrane break (between yellow lines) is evident.

without PS.^{49,55} It was even demonstrated in multivariate analysis, that PS was the most important factor of subfoveal choroidal thinning in HM.¹ Finally, Nie et al,⁵⁵ comparing AL-matched eyes with and without PS using OCT-angiography found a significant reduction in choriocapillary vascular density and deep foveal vascular density in eyes with PS.⁵⁵

Histological observations showed that the thickness and density of the choriocapillaris and the thickness of retinal pigment epithelium (RPE) and Bruch's membrane (BM) did not differ significantly between the corresponding regions in eyes with and without PS of age and AL-matched subjects.⁵⁰ However, several BM defects that spatially correlated marked scleral thinning were found within and at the edge of PS.⁵⁰ Jonas et al suggested that in these areas, accentuated eyewall stretching leads to multiple BM ruptures.⁵⁰ As the basal lamina of the RPE and that of the choriocapillaris, are components of the BM,⁵⁶ the BM-choriocapillaris-RPE complex between these ruptures retain its normal architecture.⁵⁰

A significantly thinner retinal thickness was found in myopic AL-matched eyes with than without PS.⁵⁵ Additionally, at the level of patchy atrophy, a significantly thinner thickness of all retinal layers was demonstrated.⁴⁹ Furthermore, Ohno-Matsui al³⁵ showed a reduced retinal thickness in the macula of eyes with PS. Finally, using multimodal imaging, Frisina et al found that the deepest area of the PS was characterized by a higher prevalence of chorioretinal atrophy compared to the other parts of the eye.³¹

Very recently, using in vivo triple-input polarization-sensitive-OCT in eyes with PM, Liu et al, showed that scleral collagen birefringence was associated with myopia status and was negatively correlated with refractive error.⁵⁷ Quantification of posterior scleral birefringence linked to aberrant remodeling would thus constitute a non-invasive biomarker to assess the progression of myopia.⁵⁷ Refinements of this technique are awaited.

Clinical Significance of Posterior Staphylomas

The presence of a PS is associated with a worse structural^{1,16,35,42–45,55} and functional course of HM^{1,17,19,27–29,38} potentially leading to visual impairment.

Posterior Staphyloma and Myopic Maculopathy

Chorioretinal changes were significantly more common in eyes with than without PS.^{17,25,30,38,58} They constituted the main complication related to PS,^{16–18,37} involving 77.5% of PS in the series of Curtin.¹² Similarly, An et al found that 93.3% of their patients combined PS and macular retinoschisis.²⁵ Finally, PS was significantly associated with a higher degree of myopic maculopathy (ATN myopic maculopathy classification (Atrophic/Traction/Neovascularization)),^{27,29} reaching 82% of eyes in the study of Guo et al.²⁹

Specifically, diffuse chorioretinal atrophy was significantly more common in eyes with type I PS than in eyes without a PS.¹⁷ Furthermore, among PS with macular retinoschisis, 82.1% were type I or II.²⁵ In addition, the PS compound subgroup presented a higher stage in each of the ATN components.²⁷

On the other hand, eyes with more than one protrusion presented significantly more chorioretinal atrophic lesions than those with a single protrusion.¹⁰ Additionally, myopic macular lesions were significantly more common in eyes with irregular curvature (Type I and II PS).³⁵ Finally, a significant association between the type of PS and location of chorioretinal atrophy has been reported.³¹

Interestingly, in their longitudinal study, Hsiang et al showed that despite stable AL, PS that deepened over time also developed myopic retinal degeneration.²³

Finally, eyes with PS type II and macular neovascularization had a lower depth-to-diameter ratio,⁴⁶ suggesting that type II PS might be more prone to develop macular neovascularization at a stage where the scleral protrusion is less prominent.⁴⁶

Posterior Staphyloma and Visual Function

Visual Acuity

Studies have consistently shown significantly worse mean best corrected visual acuity in highly myopic eyes with than without PS.^{12,17,25,27,29}

A wide variation in visual acuity between different types of PS^{12,17,25} Ohno 2004, has been also reported. Recent series have confirmed a poorer mean best-corrected visual acuity in PS with macular involvement (types I and II)^{25,27} as well as in the subgroup of compound PS.^{25,27}

Visual Field

Although no significant difference was observed in visual field defects (VFD) between eyes with and without PS,¹⁷ a significant difference was disclosed between eyes with PS subtype I and those without PS.¹⁷ Furthermore, eyes with more chorioretinal lesions had significantly more VFD.¹⁰ Finally, myopic eyes with VFD were found to have longer AL and irregular posterior eye contour.²⁴

In patchy atrophy at the PS edge, the location of VFD, correlated with that of retinal nerve fibers thinning over the atrophic area.⁴⁹ Park et al²⁶ found that 55.2% of myopic eyes with glaucoma-like VFD had PS and that the location of the PS (temporal or nasal to ON) was related to that of the VFD and to the direction of disc torsion.²⁶ This is consistent with previous results showing that eyes with a temporally distorted shape had significantly more VFD.¹⁰

An abrupt change in scleral curvature (types VII and IX PS) was the only factor significantly associated with VFD deteriorations observed in 73.8% of highly myopic eyes over a mean follow-up of 10 years.⁵⁹

Posterior Staphyloma and Peripapillary Intrachoroidal Cavitation

Peripapillary intrachoroidal cavitation (PICC) was found to complicate PPS in 20.5% (40/195) to 52 % (13/25) of eyes.^{20,60} The reported prevalence of PS in the presence of PICC varies between 40.2% and 100% depending on the studies.^{61,62} Recently, Ehongo et al discovered that this complication was not found in eyes with PPS in the absence of myopic conus while it was found in 22.7% of eyes combining these entities⁶⁰ (Figure 6). This co-occurrence would result from common pathogenetic factors¹³ including the ON sheaths traction force (Figure 7).

VFD have been found in up to 73.3% of PICC cases.⁶³ A correlation was noted between the distribution of these defects and the location of PICC.^{63–65} However, the mechanism underlining these deficits is not established and is suggested to be related to the degree of disc tilt.⁶⁴ These VFD raise concerns in clinical practice as they mimic glaucomatous VFD.^{63–65}

Pathogenetic Hypotheses-Discussion

So far, the etiology of PS is unknown and is suggested to be promoted by changes in the sclera.⁴⁸ In addition, thinning of the choroid and sclera related to HM and leading to secondary local decreased biomechanical resistance of the sclera is suggested.^{12,50}

Previous Hypotheses

Some theories have suggested that the thinned, weakened and more extensible sclera would protrude along the weak points. These points would correspond either to the zones of closure of the embryonic fissure,³⁵ or to the local

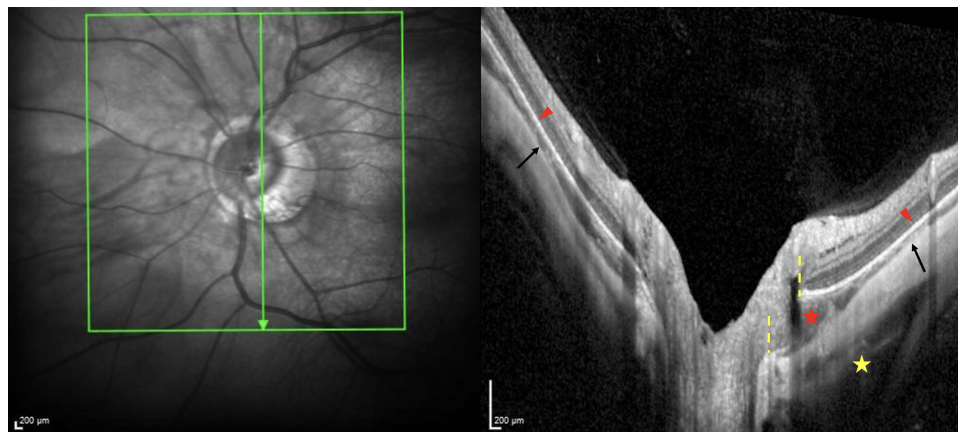


Figure 6 Peripapillary intrachoroidal cavitation. OCT section along the arrow in the infrared image. The PPS shows a gradual thinning of the choroid from the periphery towards the PPS edge (red arrowheads) and a gradual re-thickening of the choroid from the PPS edge in direction to the optic nerve. The posterior choroidal wall shows a change in the curvature radius (black arrows) at the PPS edge. The peripapillary intrachoroidal cavitation is the triangular choroidal thickening with the base against the optic nerve (red star). The yellow star is the subarachnoid space. The myopic conus is between the dashed yellow lines.

Abbreviation: PPS, peripapillary staphyloma.

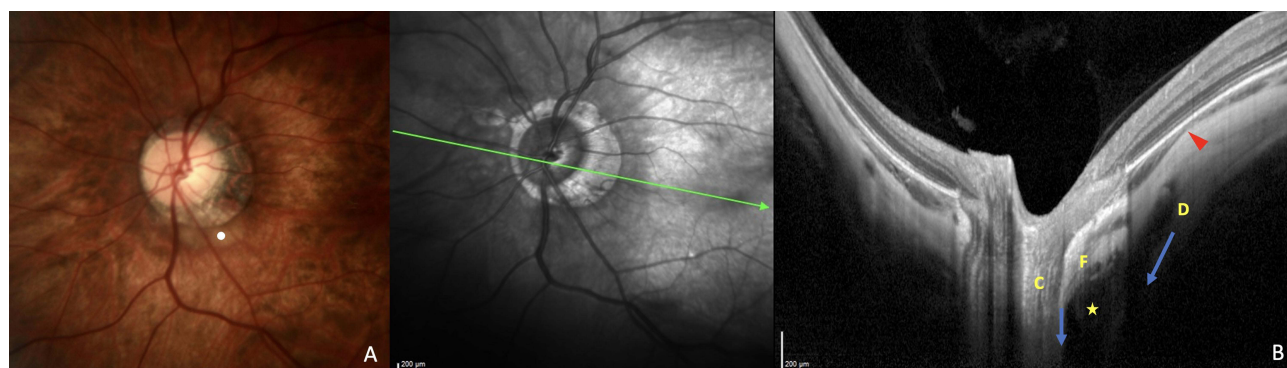


Figure 7 Pathogenetic hypothesis of peripapillary staphyloma (PPS). **(A)** Fundus image. A peripapillary intrachoroidal cavitation (white dot) is also present in this case. **(B)** OCT section along the arrow in the infrared image. The PPS shows a gradual thinning of the choroid from the periphery towards the PPS edge (red arrowhead) and a gradual re-thickening of the choroid from the PS edge towards the optic nerve and along an outwards scleral deformation. The direct posterior traction (blue arrows) exerted by the scleral insertions of the optic nerve sheaths would lead to the outpouching of the sclera while the thinning of the choroid at the PPS edge would result from the squeezing of the eyeball by the tangential component of this traction force.

Abbreviation: D, dura; F, Scleral flange; C, Lamina cribrosa; Yellow star, Subarachnoid space.

organization of collagen fibers around the ON and macula.⁴⁸ Other hypotheses suggested that choroidal thinning combined with other factors would induce scleral thinning, leading to PS.^{18,54} It was also suggested that the nonuniform defocus mechanism would trigger the occurrence of PS.¹⁶ Finally, the posterior expansion force of BM was proposed as a promoter of PS.^{18,66,67}

However, these theories do not explain the presence of PS in non-elongated eyes.^{10,11,19} Nor do they explain the pattern of outpouchings of the eye which underlies the classification of PS. Finally, all these theories suggest the hypothesis that the expansion of the eyeball would result from a driving force acting by pushing the eye wall from the inside. The possibility of a factor pulling the globe from the outside is not mentioned.

Interestingly, data from the biomechanics of the ON are evolving, allowing more and more conditions of the posterior part of the eye to be understood.

Insight from Optic Nerve Sheaths Biomechanics

Recently, it has been suggested that the traction on the sclera by ON sheaths not long enough^{39–41} to allow a full adduction may be responsible for the outward deformation of the eye leading the sclera to detach from the underlying choroid in a PICC.^{13,68} The same mechanism has been suggested for the occurrence of a PPS¹³ in which the direct posterior component of the tensile force exerted by the scleral insertion of the ON sheaths would lead to the outpouching of the sclera¹³ while the thinning of the choroid at the edge of the PPS would result from the squeezing of the choroid by the tangential component of this traction (Figure 7). Above all, as at the edge of any type of PS, OCT consistently shows a choroidal thinning, the question arises of the cause of this aspect in the other types of PS.

Compression to Potentially Explain PS Edge Features

Using 3D-MRI, Ohno-Matsui et al have shown that in PPS and type IV PS, the changes of the curvature were slight, and the eye showed a nasally distorted shape.¹⁷

They further showed that the curvature of the upper to temporal borders of the protrusion was more abrupt than that of the lower or nasal borders in the other types of PS and presented a notch-like depression.¹⁷ All eyes with type I PS had at least one notch-like depression along the temporal border (87.8%) or the upper border (56.8%) of the protrusion.¹⁷

In correlation analysis with the use of UWF fundus images, pigmentary abnormalities more obvious at the upper to temporal borders of the PS were found to correlate with the areas of abrupt changes in curvature seen at the border of PS using 3D-MRI images.¹⁷ They also matched to the choroidal thinning observed on WF-OCT sections.²⁰

This thinning of the choroid at the PS edge suggests potential localized compression, as the choroid under compression thins out.^{69,70} From these observations, I postulate that the temporal to superior part of the posterior eyeball may be subjected to a compression by the same mechanism explained for the squeezing of the choroid in a PPS.¹³

Analysis of the Insertions of Oblique Muscles on the Eyeball

The anatomic data show that, apart from the ON, oblique muscles are inserted onto the posterior surface of the eyeball: temporally and superiorly for respectively the inferior oblique (IOM) and superior oblique (SOM) muscles. Of note is the insertion of these muscles just where the compression seems to markedly apply on the eyes with PS.

Oblique muscles are unique because in addition to attaching to the posterior surface of the eyeball, they do not originate from the common tendinous ring, and they have angular attachment on the globe.⁷¹ As they may impact the curvature of the eye during their contraction and are therefore candidates as potential promoters of eyeball deformations leading over time to PS, below is a brief reminder about them.

From the trochlea in the superomedial orbital rim, the tendon of the SOM extends posteriorly and inserts onto the sclera superiorly, under the insertion of the superior rectus about 6 to 7 mm from the ON⁷¹ (Figure 8A). During incyclotorsion, it may deform the eyeball (Figure 8B). From its origin at the orbital floor just lateral to the nasolacrimal groove,⁷² the IOM continues, extends posteriorly, laterally, and superiorly. It eventually inserts on the posterior lateral surface of the eyeball (Figure 8C), close to the insertion of the SOM.⁷³ Its posterior border is 1 to 2 mm in front of the macula.⁷⁴ During the extorsion, it may also deform the globe (Figure 8D).

Link Between Oblique Muscles Dynamics, Fundus Images, OCT Findings, and 3D-MRI Features

The Arc of Contact

In primary position, each extraocular muscle has two main components regarding its eye attachments: the scleral insertion and the effective insertion.⁷⁵ The effective insertion is the point where the muscle first contacts the globe toward its route to its final scleral insertion. Each muscle thus wraps around the globe for several mm before reaching its insertion on the sclera.⁷⁵ The

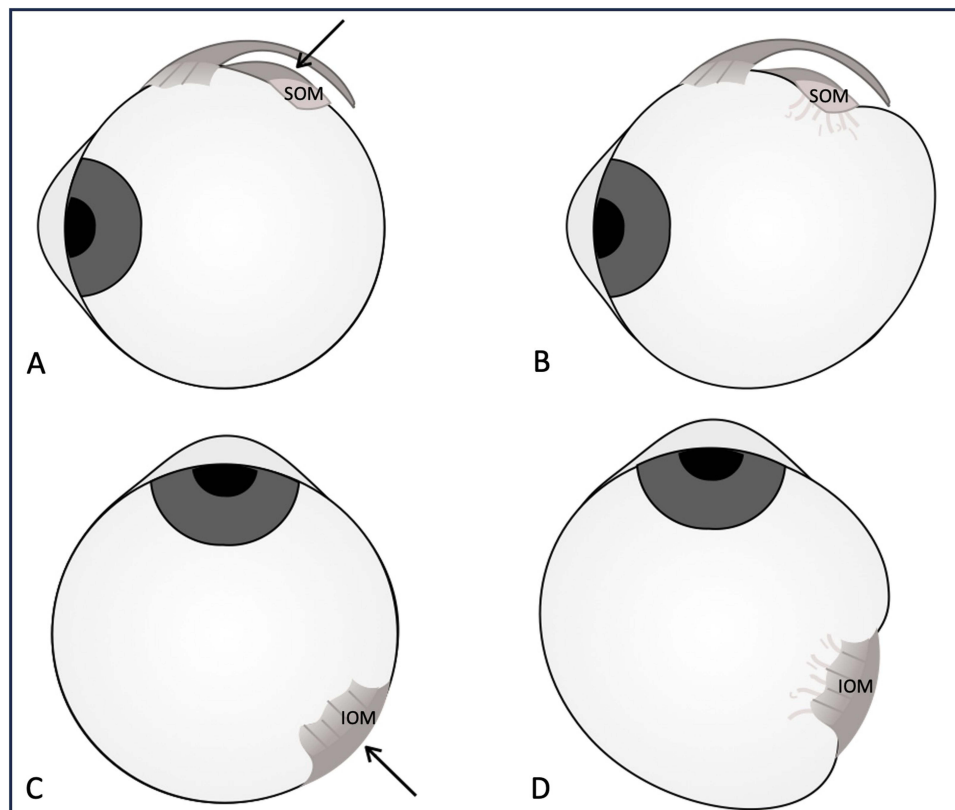


Figure 8 Hypothetical oblique muscles imprints at their insertions. Superior oblique muscle (SOM) of the left eye viewed from the temporal side at rest (A) and in contraction (B) Inferior oblique muscle (IOM) of the left eye viewed from the inferior side at rest (C) and in contraction (D). The muscles contraction push on the eyeball (black arrows), deforming it. Illustration drawn by Loïc Blommaert.

length of the muscle in contact with the globe between these two insertions is called the arc of contact.⁷⁵ The arc of contact of the IOM is 15 mm, which is the longest of all the extraocular muscles, and that of the SOM is 7–8 mm.⁷⁵

The Edge of the PS

As the muscle contracts and the eye rotates toward the muscle, the effective insertion moves toward the scleral insertion point, and the arc of contact decreases.⁷⁵ Importantly, the muscle remains tangential to the globe at its effective insertion, maintaining the same torque through much of the eye movement.⁷⁵ Due to this tangential moving contact, the eyeball may be subjected to a moving compression during the muscle contraction all along the arc of contact of the muscle.

By applying this to the IOM, the temporal part of the eyeball would thus be subjected to a compressive action which could then lead to the temporal edge of the PS, corresponding to pigmentary anomalies seen on ophthalmoscopy^{11,17,20} (Figure 9A). The same analysis is valid for the SOM for the upper edge of the PS.



Figure 9 Wide macular posterior staphyloma (PS) - (Type I PS). I-Characteristics. (A) Right fundus image. The edge of the PS shows pigmentary abnormalities (arrowheads). Arrows indicate the WF-OCT sections in (D) and (E). (B and C) 3D-MRI viewed from the inferior (B) and nasal (C) sides. The arrowheads show the borders of the PS. (B) The arrow points to a notch at the temporal border. (D and E) WF-OCT sections. Horizontal (D) and vertical (E) scans showing an inward protrusion of the sclera with a thinning of the underlying choroid (white arrows) at the edge of the PS, followed by an outwards deformation of the sclera towards the posterior pole. (F and H) 3D WF-OCT images viewed from the anterior (F), nasal (G), and inferior (H) sides, disclosing the borders (arrowheads) of the PS and the notch (arrows) in (G) and (H) at the border of the PS. This illustration is used with the permission from IOVS and corresponds to Figure 2 of Shinohara et al²⁰ 2- Hypothetical muscles involvement on PS characteristics. The horizontal arrow in (A) crosses the temporal border of the PS and provides information on the possible involvement of the inferior oblique muscle: pigmentary abnormalities on fundus (A), notch in the temporal border (B and H), inward deformation of the eyeball (D). The vertical arrow in (A) crosses the upper border of the PS and provides information on the possible involvement of the superior oblique muscle: pigmentary abnormalities on fundus (A), inward deformation of the eyeball (E) and the notch in the upper border (G).

Notes: Reprinted with permission from Shinohara K, Shimada N, Moriyama M, et al. Posterior Staphylomas in pathologic myopia imaged by widefield optical coherence tomography. *Invest Ophthalmol Vis Sci.* 2017;58(9):3750–3758.²⁰

Abbreviations: WF-OCT, widefield optical coherence tomography; 3D-MRI, Three-dimensional magnetic resonance imaging; 3D WF-OCT, Three-dimensional optical coherence tomography.

If we perform a correlation analysis with the use of 3D-MRI images, this could explain why the upper to temporal margins of PS are more abrupt¹⁷ (Figure 9B and C).

These edges of PS were also found to show a choroidal thinning on WF-OCT sections (Figure 9D)²⁰ as well as an inward deformation of the sclera towards the vitreous.²⁰ Vertical OCT section of (Figure 9E) corresponds to the same analysis for the SOM.

Finally, 3D WF-OCT provided high resolution tomographic reconstructions of PS, viewed respectively from the anterior (Figure 9F), nasal (Figure 9G), and inferior (Figure 9H) sides. Figure 9 is used with the permission from IOVS and corresponds to Figure 2 of Shinohara et al.²⁰

The Notch-Like Depression of PS

The IOM could compress the eyeball at the limits of its insertion as it has been suggested for the PPS¹³ and eventually lead over time to the temporal notch observed in 3D-MRI (Figure 9B). Same analysis for the upper notch observed on 3D-MRI in the upper part of the eyeball, in relation to the insertion of the SOM.

The Shape and Type of PS

The compression at the arc of contact of the IOM separates the globe into two parts in the anteroposterior axis. The eyeball portions at the anterior and posterior borders of the arc of contact of the IOM are free of its compressive action and would show outpouching on either side of the compressive area (Figure 10A–D).

However, as the ON sheaths also pull significantly on the peripapillary area via their attachments,⁶⁹ they also deform the eyeball as already stated¹³ (Figure 10E–H). The posterior part of the eye is thus subjected to this additional force (Figure 10K–L).

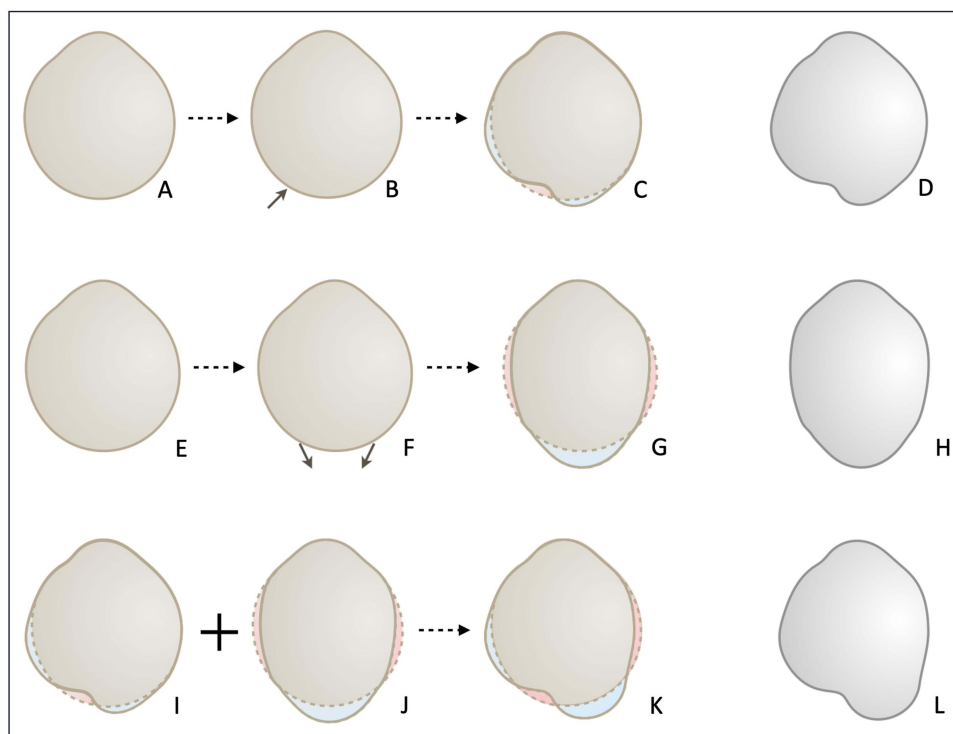


Figure 10 Hypothetical pathogenesis of posterior staphylomas (PS). (A–D) The eye (A) subjected to the compression of an oblique muscle during its contraction (B) undergoes a deformation (C) corresponding to outpouchings (blue areas) on either side of the contact area (pink zone) which deforms inwards under the compression, leading to its final shape (D). When the same eye (E) is subjected to the traction of optic nerve sheaths (F), it deforms (G), and presents an outward protrusion (blue area) and a “pinch” (pink areas) at the end of the traction area, at the either side of the protrusion, leading to its final shape (H). As the eye is normally subjected to both forces (I and J), it combines the changes resulting from each component (K), leading to its final shape (L) which is that of the PS and corresponds to the interaction between the different forces. Illustration drawn by Loïc Blommaert.

The final appearance of the posterior protrusion of the eye would then be dictated by the sum of these forces (Figure 10L). Over time, repetition of these deformations would lead to tissue remodeling and permanent fixation of these deformities, corresponding to PS. The same analysis applies for the SOM.

In (Figure 11), used with the permission from IOVS, and corresponding in part to Figure 4 from Shinohara et al,²⁰ a PS shows pigmentary abnormalities on the fundus (Figure 11A), matching to its edges as seen on 3D-MRI images, which additionally show a temporal notch (Figure 11B and C).

Analysis of Potential Forces at Play

IOM: the horizontal WF-OCT section shows an anterior protrusion at the temporal edge of the PS (blue arrow, Figure 11D) potentially induced by the IOM. One would expect to observe an outward deformation of the eyeball at either side of this inward deformation induced by this muscle, which is the case and begins at the level of the blue arrowheads in Figure 11D. A corresponding thinning of the choroid along the inward deformity (white arrows,

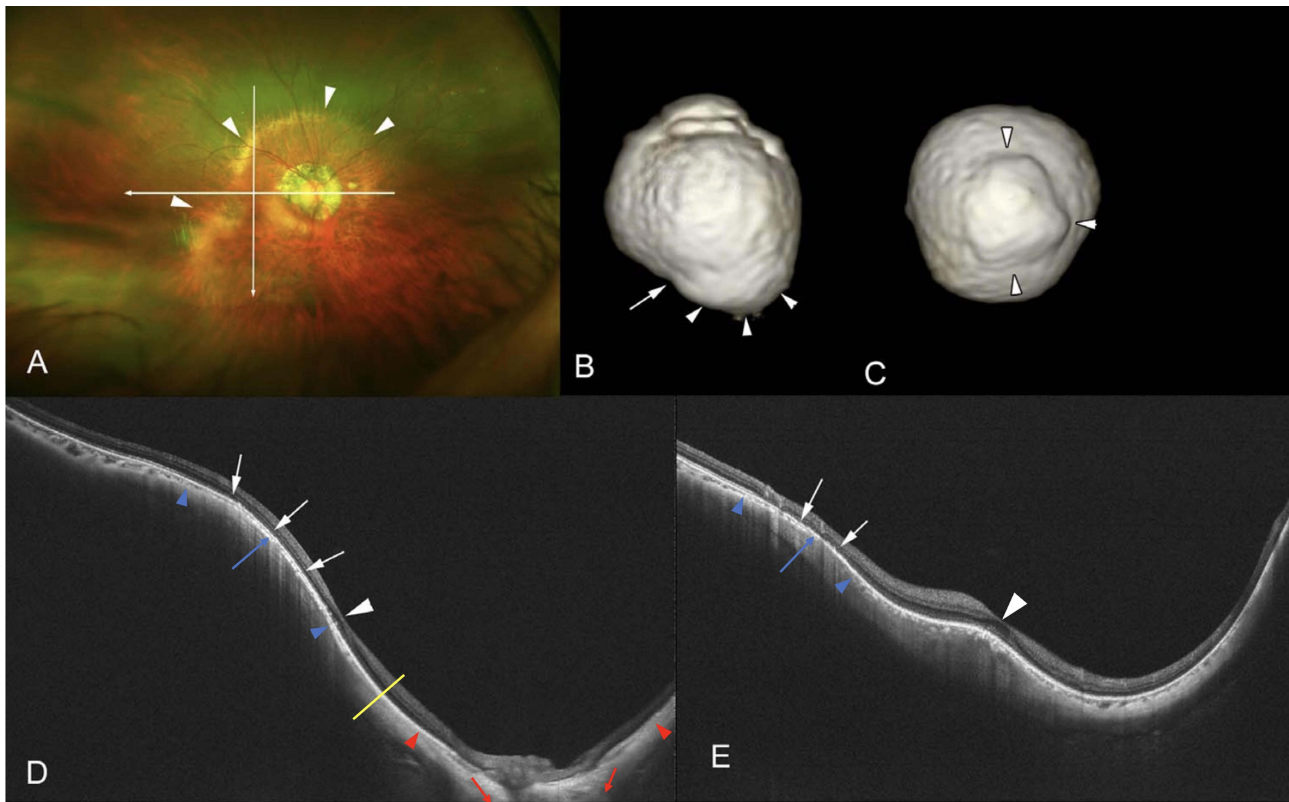


Figure 11 Posterior staphyloma (PS) (type VI of Ohno-Matsui classification). 1- Characteristics. (A) Right eye fundus showing pigmentary abnormalities at the border of a wide PS (arrowheads). Arrows indicate the scanned lines of WF-OCT sections in (D) and (E). (B and C) 3D-MRI viewed from the inferior (B) and posterior (C) sides, showing the border of the PS (arrowheads). In (B), the posterior outpouching is located nasally; however, different from a peripapillary staphyloma, the outpouching has a wide opening angle leading it to be classified as “other”. Also, a notch is located at the temporal border of the PS (arrow). (D and E) Horizontal (D) and vertical (E) WF-OCT sections. An inward protrusion of the sclera and a thinning of the choroid are located at the edge of the PS both in the horizontal and vertical sections (white arrows). A posterior displacement of the sclera follows the inward deformation toward the posterior pole. In (D), the fovea (white arrowhead) is located on the slope of the PS nasal to the PS edge, and the optic nerve head is located at the bottom of the PS. (E) A posterior scleral displacement in the lower fundus with a dome-shaped appearance of the macula (white arrowhead) are shown. This PS was classified as “other” (peripapillary and inferior type) by WF-OCT. This illustration is used with the permission from IOVS and corresponds to Figure 4 of Shinohara et al²⁰ 2- Analysis of potential muscles and optic nerve sheaths involvement on PS characteristics. (D) Section along the horizontal line. The anterior protrusion at the temporal edge of the PS (blue arrow), would result from the indentation of the IOM, with outward deformation of the eyeball on either side (blue arrowheads). The corresponding thinning of the choroid along the inward deformation (white arrows) and rethickening of the choroid beginning at the end of the inward deformation (blue arrowheads) toward the posterior pole are seen. (E) The same analysis for the upper edge about the SOM. Also, in (D), around the optic nerve head: an outward deformation resulting from the traction of its sheaths is perceived (red arrows). Although the choroid is thin, it nevertheless presents a slight thickening in front of this outward deformation. Next, the choroid shows a thinning at the site of the pinching of the meningeal sheaths (red arrowheads). This thinning meets on its way (yellow line) the re-thickening (from the blue arrowhead) due to the action of the IOM. This case illustrates that the final shape of the eyeball results from several interactions.

Note: Reprinted with permission from Shinohara K, Shimada N, Moriyama M, et al. Posterior Staphylomas in pathologic myopia imaged by widefield optical coherence tomography. *Invest Ophthalmol Vis Sci.* 2017;58(9):3750–3758.²⁰

Abbreviations: WF-OCT, widefield optical coherence tomography; 3D-MRI, Three-dimensional magnetic resonance imaging; IOM, Inferior oblique muscle; SOM, superior oblique muscle.

Figure 11D) and re-thickening of the choroid beginning at the end of the inward deformity (blue arrowheads, Figure 11D) is seen as expected.

ON sheaths: around the ON head, the eyeball exhibits an outward deformation due to the direct traction forces of the ON sheaths (red arrows, Figure 11D) which is followed by the pinching of the choroid induced by the tangential component of the pull of these meninges (red arrowheads, Figure 11D). The posterior outward deformation due to the IOM (with the corresponding choroidal re-thickening) crosses this choroidal compression in its path (yellow line, Figure 11D).

The final appearance of the eyeball depends on the importance of each force (muscles and ON sheaths) (Figure 11B). This PS was classified as other = type VI (Ohno-Matsui's classification) by Shinohara et al,²⁰ with PPS constituting one of its components.

SOM: Along the same line, the vertical WF-OCT section (Figure 11E) shows that the inward deformation with related components of this PS at its upper edge would result from the action of the SOM.

Nasal side of the eyeball: eyes with PS show less deformities on the nasal side¹⁷ (Figures 9B and 11B), fitting with the fact that this part of the eye is not in contact with oblique muscles and is therefore less impacted by their contraction forces.

The IOM is a band about 9 mm wide and thus has an anterior and posterior edge.⁷³ It is slender and has two surfaces: ocular and orbital.⁷⁴ According to the main positioning of the tangential forces (at its anterior or posterior edge) along its arc of contact, their amplitude and their extent, the impact on the globe would lead to the appearance of PS type I or II which are the more frequent.^{12,17,23,25}

The pathogenesis of PPS has previously been suggested¹³ (Figure 7).

The distribution of the traction forces of the ON sheaths differently on their scleral attachment, combined with the action of the oblique muscles would lead to the appearance of several types of PS, which need further investigation.

Moreover, since the impact of the meningeal sheaths is not limited to a single axis due to the orientation of the ON from the orbit towards the eyeball, and since the properties of the sclera would also act, there are several interactions determining the appearance of deformities of the eyeball.

Finally, depending on the position of the eye, SOM additionally, allows it to move down and out while IOM is also responsible for elevation, and abduction. Therefore, how these muscles would compress or pull on the eyeball would depend on the movement involved and the starting position of the eye for that specific movement.

The eyeball would thus be permanently and according to the eye movements, subjected to different forces which would induce intermittent deformations of its wall. The resultant of these forces over time would determine the shape and the location of potential protrusions and explain why the types of eyes deformities are numerous,^{10,11,16} and more complex than current classification.⁷⁶ Moreover, this would also explain the existence of compound types of PS, the precise diagnosis of which is best made using WF imaging (Figure 12A and B).

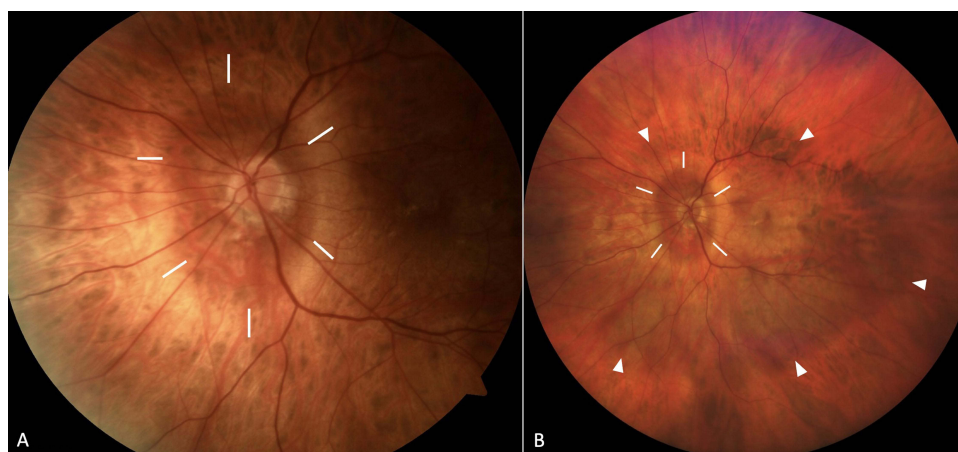


Figure 12 Fundus image of Type VI PS (Ohno-Matsui), corresponding to Curtin type VII: Peripapillary staphyloma (PPS) and wide macular staphyloma. **(A)** In 50° imaging by Visucam®, only the PPS is obvious. White lines outline its edges. **(B)** In 240° imaging with Clarus® the outermost edges (white arrowheads) of a wide macular posterior staphyloma are discloses, revealing its compound nature and emphasizing that the accurate diagnosis of PS is best made using wide-field imaging.

Interestingly, in eyes with HM, using 3D-MRI, a recent work disclosed deformities at the equatorial part,⁴⁷ which warrants further investigations as these deformities could be related to the impact of the rectus muscles on the eyeball.

The reduced tissue resistance in HM^{42,44,45} would explain why PS are more common in this refractive group. Finally, the gradual and acquired nature of these changes would explain their high prevalence with aging.^{12,17,21,23,27,29,35}

Recently, significant gaze-induced globe deformations in eyes with PS were demonstrated in all gaze positions by 3D-MRI.⁷⁷ Moreover, the increase in the vitreous chamber axial volume occurred specifically in downgaze,⁷⁷ supporting the association of near activities with myopia occurrence and progression⁷⁷ and warranting further confirmation.

Table 2 summarizes the main developments in the knowledge of PS.

Quantitative Aspects – Long-Term Changes

A quantitative approach would allow standardization of PS characteristics for large-scale studies.

The Shape of Staphyloma

Using 3D WF-MRI, Moriyama classified the ocular shapes of eyes with HM into 4 distinct types: nasally and temporally distorted, cylindrical, and barrel-shaped.¹⁰ Interestingly, the deformations related to the present hypothesis (Figure 10A–L) fit with these shapes.

By analyzing the outer and inner scleral curvatures with a combination of 3D-MRI and SS-OCT, Ohno-Matsui et al found that all temporally distorted eyes on 3D-MRI showed irregular scleral curvature on OCT and all eyes with temporal slope and irregular curve on OCT had a PS.³⁵

Quantitative analysis of mean scleral local curvature and its variance in eyes with PS with SD-OCT showed that they were greater in female, elderly, and eyes with longer AL, implying that these groups had less “smooth” and therefore more severe curvature of the eye. These parameters provide an indication of the severity of PS.²¹

The Depth of Staphyloma

Curtin had already noticed that PS type II was shallow, with the steepest margins at the disc.¹² Then, UWF-OCT confirmed that PS type II was significantly deeper than type I, with abrupt margins, and was therefore not a smaller version of type I.⁴⁶ Additionally, unlike PS type I, its depth-to-diameter ratio correlated with AL, meaning that eyes with longer AL have more severe PS type II.⁴⁶

As a significant positive correlation between PS depth and width was found,^{12,23,31,35} it was suggested that over time, PS diameter and depth increase simultaneously.²³

However, very recently, UWF-OCT showed that the depth-to-diameter ratio increases with age, implying that the PS deepens more than it widens with age,⁴⁶ thus confirming its increasing severity with age.²¹

Long-Term Changes

Paving the way for understanding PS, Curtin classified it into 10 subtypes.¹² Interestingly, all primary types except type I are related to the ON head (Figure 13 Columns A–C). Moreover, as just discussed, the severity of PS increases with age: it deepens^{12,31,35} and becomes irregular over time.^{21,23}

Furthermore, as previously discussed, (Table 1) among the 3 OCT criteria for the diagnosis of PS,²⁰ Tanaka et al showed that the inward protrusion of the sclera at the PS edges was not the earliest, being absent in some slight cases.³⁶ This is consistent with Curtin’s results showing that sharp-edged PS are unusual in the youngest age group.¹² Therefore, Tanaka et al suggested that later, when the PS deepens, an inward protrusion of the sclera at its edges then occurs.³⁶

Although PS types I and II are consistently the most common,^{12,17,23,36} Curtin showed that PS type II, the 2nd most frequent in patients aged 3–19 years, became less frequent in older subjects¹² (Figure 13 Column D). Moreover, he found that compound types were more common in older subjects,¹² which recent findings confirm.³¹ The increasing complexity of PS with age was established by Hsiang through a longitudinal observation of some PS moving from type II to type IX over 20 years.²³

Table 2 Main Developments in the Knowledge of Posterior Staphyloma

Year Author (Ref)	Objective	Method	Results	Strength	Drawback
1801 Scarpa ¹⁵	1st description of PS.	A pair of post-mortem eyes.	Identification of posterior staphyloma as an entity.	1st description of PS.	Post-mortem
1977 Curtin ¹²	To determine morphologic types of PS, their prevalence, and their effect on visual acuity.	Fundus stereoscopic ophthalmoscopy and drawings.	Ten types of PS, 5 primary and 5 compounds.	1st classification of PS.	Subjective, complicated.
1999 Takano ⁵⁸	To evaluate OCT features of the retina in eyes with severe myopia and PS.	TD-OCT.	Foveal retinal detachment and retinoschisis found in eyes with PS.	Foveal retinal detachment and retinoschisis are common in PM with PS.	Conventional OCT imaging is limited in depth and extent. TD-OCT is obsolete.
2008 Hsiang ²³	To analyze the relationship between grade/type of PS and incidence of myopic macular lesions.	Ultra-sound A and B. Follow up of some PS over 20 years.	90% of eyes with HM had PS. Morphologic features of PS worsen with age. Deep PS are related to more severe myopic maculopathy.	Longitudinal analysis of 9 eyes over 20 years showing that PS deepens with age. Transition of some type II PS to type IX PS.	Only 2D images generated.
2011 Moriyama ¹⁰	To image the entire shape of the eye.	High-resolution volume rendering 3D-MRI.	The entire eye in pathologic myopic eyes divided in 4 distinct shapes: nasally and temporally distorted, cylinder and barrel. Temporally distorted eyes had more visual field defects. Eyes with ≥ 2 protrusions had significantly more chorioretinal lesions than eyes with ≤ 1 protrusion.	1st analysis of the whole shape of the eye. Capture of the entire large PS. The shape of the eye correlates with myopic complications in PM.	3D-MRI is not available in routine clinical settings. Slight curvature changes not detected by 3D-MRI.
2013 Henaine-Berra ³⁰	To determine the prevalence of macular complications in eyes with high myopia and PS.	SD-OCT.	Macular abnormalities significantly more common in eyes with PS.	Visualization of retina, choroid, and the anterior scleral contour.	Conventional OCT imaging is limited in depth and extent.
2012 Ohno-Matsui ³⁵	To analyze the shape of the sclera determined by SS-OCT and to correlate it with myopic retinochoroidal lesions.	SS-OCT and 3D-MRI.	Scleral curvature irregularities are more common with age and longer AL. All the eyes with temporal slope and irregular curve on OCT had PS.	Myopic fundus lesions significantly more common in eyes with irregular scleral curvature.	The posterior scleral contour could not be captured in all the eyes by SS-OCT.

(Continued)

Table 2 (Continued).

Year Author (Ref)	Objective	Method	Results	Strength	Drawback
2014 Spaide ¹⁶	To determine the definition of PS.	Criteria defining a PS based on curvature were established.	PS is an outpouching of a portion of the wall of the eye with a radius of curvature lesser than that of the adjacent zone.	Unequivocal uniform definition of a PS based on curvature.	Not all PS have sharp change of curvature in their edges.
2014 Ohno-Matsui ¹⁷	To determine the incidence and types of PS using 3D-MRI. To correlation 3D-MRI and fundus features of PS.	3D-MRI and ultra-widefield (UWF)-fundus images IR and AF images and size of PS.	6 types of PS, 5 primary and type VI that is made of all the compound PS. Correlation between 3D-MRI and fundus features of PS.	Criteria defining a PS based on UWF-fundus photos were established. Simplified classification of PS.	Subtle changes of curvature (types III and IV) not detected by 3D-MRI (low spatial resolution).
2016 Shinohara ¹⁹	To analyze morphologic features of peripapillary staphyloma (PPS; type III PS).	SS-OCT and indirect ophthalmoscopy.	Definition of OCT features of PPS. SS-OCT has a high resolution enabling to detect type III and IV PS and to analyze choroid and retina.	1st study analyzing PPS (type III PS).	Caution should be paid not to miss compound PS with conventional OCT acquisition.
2017 Shinohara ²⁰	To diagnose PS using 3D rendering widefield SS-OCT (WF-OCT) and 3D-MRI.	Comparison between 3D-MRI and a WF-OCT Prototype, the multiple scan lines of which allow scan maps for 3D reconstruction of PS.	Good concordance between WF-OCT and 3D-MRI. PS has 3 key OCT features: a gradual choroidal thinning toward the PS edge, an inward protrusion of the sclera at PS edges, an outward protrusion of sclera in the area posterior to PS edges.	Imaging of very large or deep PS allowing accurate diagnosis of PS and detection of the extent of PS. 3D-WF-OCT Provides 3D images of region of interest.	Prototype, not available in clinical settings.
2019 Tanaka ³⁶	To determine first signs of PS in highly myopic eyes of young subjects.	Wide-field OCT.	In the early stage, the inward scleral deformation at the edge of a PS may be absent. PS shows then a gradual thinning of the choroid toward the PS edge and a gradual re-thickening of choroid from the PS edge toward the posterior pole along with the outward scleral deformation.	Choroidal thickness changes and the scleral outward deformation constitute the early signs of the PS edges.	Cross-sectional study.
2023 Hoang ⁷⁷	To assess gaze-induced axial volume change in eyes with posterior staphyloma	3D-MRI imaging with eye gaze in 5 directions: primary, N, T, S and I. Comparison between the primary position and each of the other directions.	Significant globe deformation was noted in all gazes. Vitreous chamber axial volume increased only in downgaze.	First study showing in vivo change in vitreous chamber axial volume. This could be relevant for the impact of near work on myopia onset and progression.	Procedure to refine and improve. Correlation analysis with myopia progression and longitudinal analyses wanted.

2022 Nakao ⁴⁶	To determine the shape of PS and identify factors contributing to the shape and grade of PS. To compare PS type I and II.	Ultra-wide-field OCT. Types I and II PS were compared. Maxi depth-to-Maxi diameter ratio.	AL was significantly longer in Narrow PS and was correlated to depth-to-diameter ratio. Age was significantly correlated with depth-to-diameter ratio in both types I and II PS. Type II PS was significantly deeper than type I PS.	Quantitative evaluations of the shape and the depth of PS to monitor their progression and evaluate the risk of damaging the retina	Cross-sectional study.
2022 Ehongo ¹³	To study the pathogenesis of peripapillary myopic changes.	Spectral Domain-OCT.	PPS is suggested to result from traction force of the optic nerve sheaths at their scleral insertion.	Traction/compression on eyewall may promote PPS.	Cross-sectional study. WF-OCT not used.
2023 Liu ⁵⁷	To measure posterior scleral birefringence as a biomarker of scleral changes.	Triple-input polarization-sensitive-OCT.	In a cross-sectional study involving adults, scleral birefringence was associated with myopia status and negatively correlated with myopia.	Collagen birefringence analysis may constitute a biomarker of scleral changes.	Procedure to refine and improve.
2023 Luo ⁴⁷	To assess global ocular deformation in pathologic myopia.	High resolution 3D-MRI.	The equatorial part of the eye also shows deformations.	Ocular deformations in pathologic myopia affect the entire eye. This is relevant in the pathogenesis of PS.	The necessity of 3D-MRI precludes its use in clinical settings.

Abbreviations: PS, Posterior staphyloma; 2D, Two-dimensional; 3D, Three-dimensional; MRI, Magnetic resonance Imaging; OCT, optical coherence tomography; UWF, ultra-widefield WF-OCT, widefield optical coherence tomography; 3D-MRI, Three-dimensional magnetic resonance imaging; TD-OCT, time domain optical coherence tomography; SD-OCT, spectral domain optical coherence tomography; SS-OCT, swept source optical coherence tomography; AL, axial length; N, nasal; T, temporal; S, superior; I, inferior.






A	B	C	D
Type of posterior staphyloma	Schematic landmarks of PS based on ONH	Type of ONH-PS relationship	Prevalence of PS by age group 3-19 vs 60-86 years
I		ONH within the PS	Decrease (26.1 vs 22.1%);249 eyes
II		ONH in contact with the PS	Decrease (73.7 vs 10.5%);38 eyes
III		ONH in the center of the PS	Increase (28.6 vs 71.4%);7 eyes
IV		ONH in contact with the PS	Increase (9.1 vs 59.1%);22 eyes
V		ONH in contact with the PS	Increase (33.3 vs 50%);12 eyes

Figure 13 Data analysis of posterior staphylomas (PS) retrieved from Curtin.¹² Column (A) Types of PS (I to V) according to Curtin's classification. Column (B) Landmarks of PS with respect to optic nerve head (ONH), based on Curtin's drawings. Black curve: optic nerve. Black cross: macula. Green curve: boundaries of PS. Column (C) Relationship between PS and ONH. It defines the location of PS edge with respect to the ONH. (B and C) There is a close relationship between most PS edges and the optic nerve. Column (D) the prevalence of PS for the two groups of age. Calculated from Curtin's Table II. Curtin.¹² All the PS except Types I and II, already more frequent in young subjects, increase with age.

Abbreviation: PS, posterior staphyloma; ONH, optic nerve head.

This suggests that, under the influence of promoters, the type of PS expressed first reflects the impact of the strongest promoter. Over the time, the primary deformation becomes more pronounced, and the effect of the weaker promoter eventually becomes apparent, leading to compound subtypes.

Interestingly, the transition noted by Hsiang²³ was from type II to type IX, whereas PPS, known for its subtle margins¹⁷ can easily be underdiagnosed.

Figure 14 shows that type IX could reflect a combination of a PPS (Figure 14A) and type II PS (Figure 14B). The septum (Figure 14C) would therefore correspond to the meeting point of their respective temporal (Figure 14D) and nasal (Figure 14E–14F) edges. Some PS types IX would therefore have been initially misdiagnosed as type II until the accentuation related to the scleral elevation at the edge of PPS allowed the diagnosis to be refined. This would explain the increase in prevalence of type IX while that of type II decreases over time.¹²

OCT photomontage (Figure 15A) provides the WF-OCT equivalent of this type IX PS whose hypothetical composition is schematized in (Figure 15B). Wide-angle OCT scans (Figure 15C and D) clearly reveal that the ridge between the two constituent components is related to the ON sheaths. The hypothetical promoting ON sheaths traction forces are presented in (Figure 15E and F). Figure 16A shows the UWF photo of this PS type IX. The upper and lower edges of its PPS-component are shown in Figure 16B and C respectively.

This discussion of the constituent elements of the combined PS suggests the progressive deformation of the eyeball under the simultaneous action of numerous forces, including traction of the ONH sheaths (Figures 11 and 15). As most PS, including primary types¹² (Figure 13 Columns A–C) are in close relationship with the ONH, whose sheaths would contribute to their emergence, the pathogenetic analysis of PSs should therefore involve the ONH.

Posterior Staphyloma. Treatment, Prevention, Perspectives

Since PS is the main determinant of visual impairment in eyes affected by HM and many unknowns remain regarding its understanding, management and prevention of myopia constitute the core of its prevention.

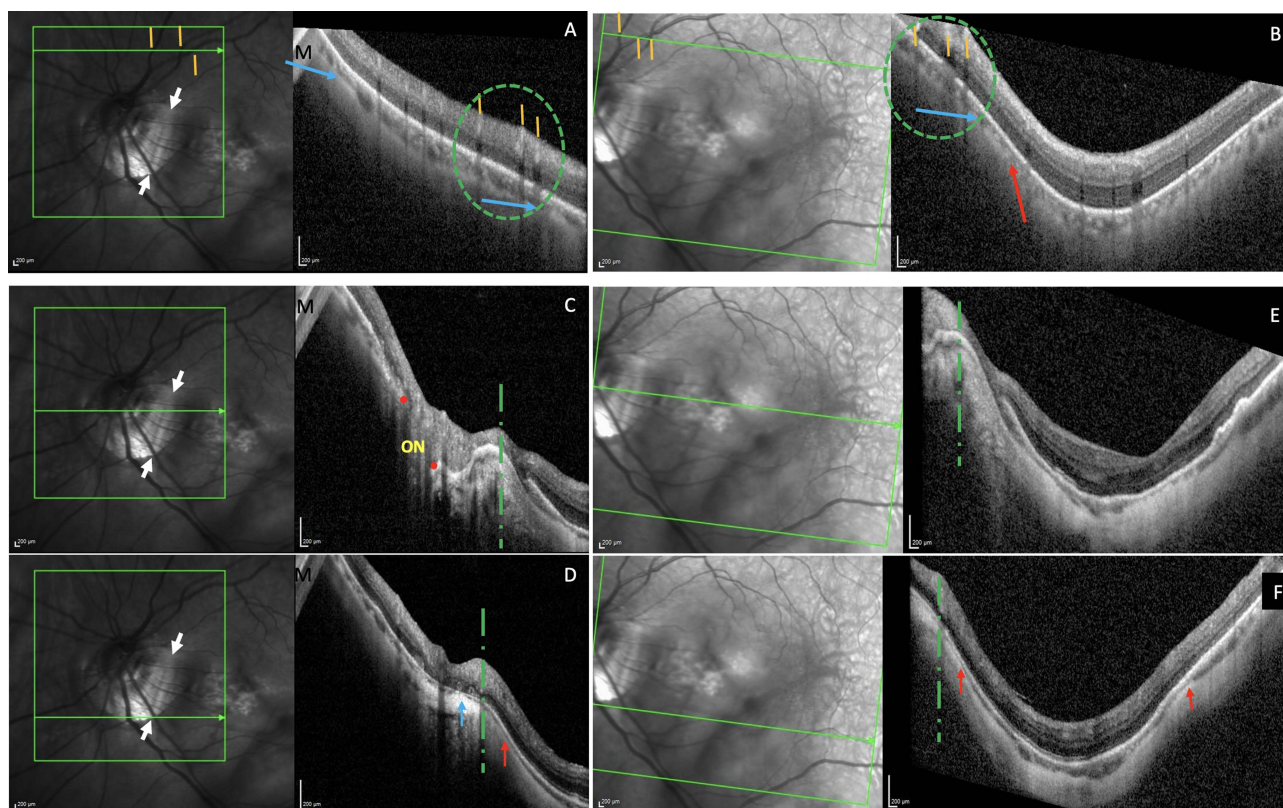


Figure 14 Posterior staphyloma (PS) type IX (Curtin classification). Analysis of its constituent components. **(A)** Linear OCT section along the green arrow in the infrared image. The section is in the upper peripapillary area and discloses a peripapillary staphyloma (PPS) whose ends are indicated by the blue arrows. **(A and B)** the green dashed circle indicates the zone of junction between sections **(A)** and **(B)**. The yellow bars highlight the superior temporal vessels constituting landmarks to reconstruct the shape of this posterior pole. **(A, C and D)** The white arrows in the infrared images indicate the ridge. **(B)** Temporal continuation of the section presented in **(A)**. The transition between the two components of this PS is highlighted by the blue arrow for the end of the PPS and the red arrow for the beginning of the 2e component. **(C)** Section across the optic nerve (ON) head as shown on the infrared image. The red dots indicate the opening of the scleral canal. **(C–F)** The dashed green lines indicate the transition zone of the 2 constituent components of this PS which is located at the ridge (detailed analysis of the ridge is presented in **Figure 15**). **(D)** This section encompasses the transition between the two components of this PS; The blue arrow indicates the end of the PPS. The red arrow shows the beginning of the 2e part of this PS. **(E)** This section encompasses the temporal continuation of section **(C)**. **(F)** The edges of the 2e component of this PS are captured and indicated by the red arrows. In total, this compound PS is made by a combination of a PPS and type II PS which meet at the ridge.

Early-Stage of Myopia

Measures to prevent the onset of myopia by encouraging children's outdoor activities and reducing near-work are effective.^{78,79}

Progression of Myopia

Low-dose atropine, orthokeratology and peripheral defocusing corrections are effective in controlling myopia progression.^{80,81} Their side effects and complications are known.^{82,83} Combined treatments appear more effective than monotherapy^{84,85} and are under investigation.^{86,87}

Complications of Myopia

Each complication of myopia is managed according to standards of care (choroidal neovascularization, traction maculopathy, retinal detachment, glaucoma...). However, the prognosis is limited in most cases and no solutions are available for chorioretinal atrophy, non-glaucomatous neuropathy and PS. Nonetheless, options for addressing the scleral outpouching of PS are summarized below.

Reshaping the Sclera in Posterior Staphyloma

Posterior scleral reinforcement for PS involves surgical implantation under general anesthesia of donor sclera, lyophilized dura or other materials^{88,89} to strengthen the posterior eyewall directly and mechanically. This procedure requires further studies to confirm its usefulness, safety⁸⁹ and long-term results.⁹⁰

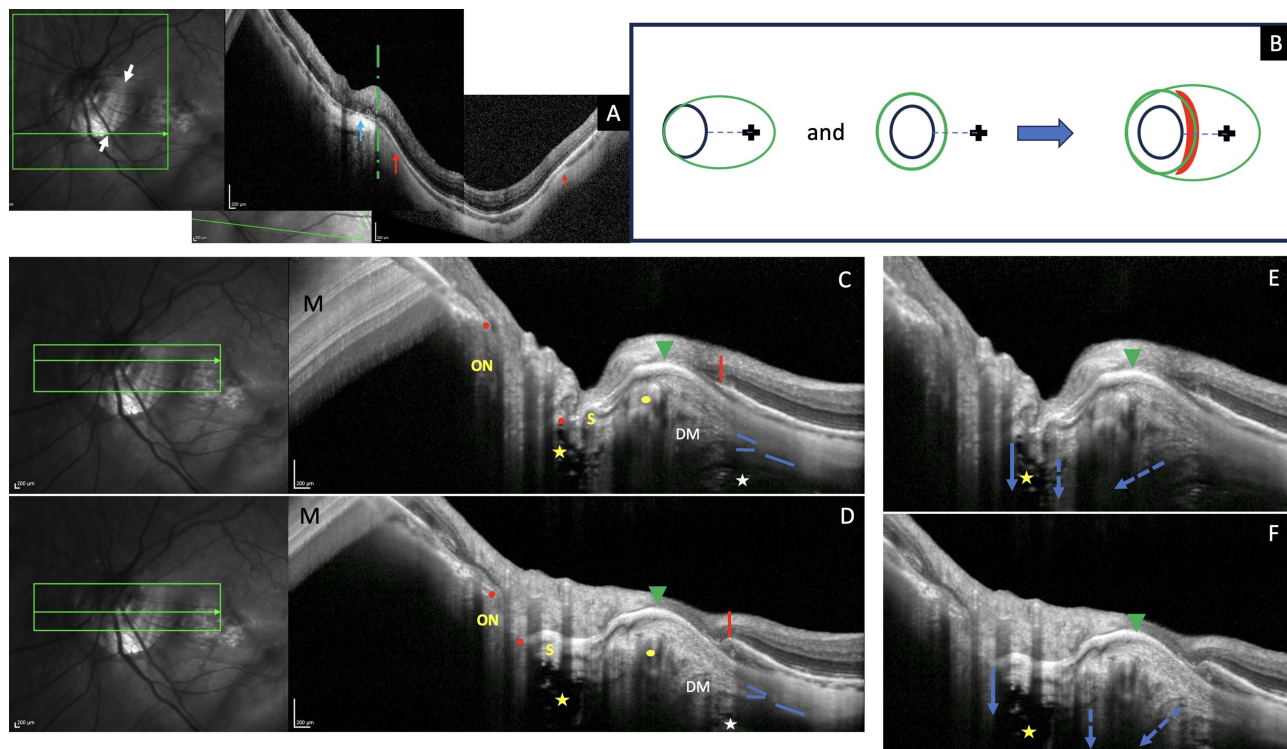


Figure 15 Posterior staphyloma (PS) type IX. Analysis of its hypothetical pathogenesis. **(A)** This image is a montage of parts **(D)** and **(F)** of Figure 14 and constitutes the equivalent of a widefield OCT. The ridge, pointed out by white arrows in the infrared image, is an inward protrusion (green dashed line) of the eye wall and corresponds to the concomitant ends of the two components of this compound PS (blue and red arrows). **(B)** Schematic pathogenetic analysis of the constituent elements of this compound PS. Black curve: ON. Black cross: macula. Green curve: boundary of each staphyloma. Red crescent: the ridge of type IX PS. **(C and D)** OCT sections along the green arrow in the corresponding infrared images. The sections are across the optic nerve (ON). The ridge is an inward protrusion (green triangles) of the wall of the eye and corresponds to the concomitant ends of the two components of this compound PS. **(C)** and **(D)**. The ridge is in front of the dura mater (DM) which fibrillar aspect is disclosed by variation in reflectivity. The gamma-delta zone corresponding to the peripapillary area free of Bruch's membrane between the red dot and the red line is extended and deformed inward. The scleral flange (**S**) is posteriorly deformed. The 3 blue bars indicate the transition at the scleral insertion of the dura (DM). Red dots: the scleral opening. Yellow dots: the arterial circle of Zinn-Haller. White star: retro-orbital fat. Red line: end of Bruch's membrane. **(M)** mirror artifact. **(C–F)** Yellow star: subarachnoid space. **(E)** and **(F)** are respectively portions of sections **(C)** and **(D)**, labelled with the hypothetic traction of ON sheaths. Dashed blue arrows: DM. Blue arrow: pia mater.

Scleral cross-linking involves the formation of bonds between collagen polymer chains to stiffen the sclera. It shows promise in reshaping the eyeball by halting the aberrant scleral remodeling. Strategies involving either light energy or chemical processes are at different stages of translational development.^{91–93}

Fibroblast transplants performed on the sclera in a rat model of deprivation myopia⁹⁴ provided a significant reduction in ocular elongation and myopic shift in transplanted compared to non-transplanted eyes. Further results are awaited.⁹⁴

Insights from Recent Data on Myopia in Humans

Curvature irregularity²¹ and depth-to-diameter ratio⁴⁶ are quantitative parameters for assessing PS severity. Gaze down movement, unlike other gaze directions was found to increase the axial volume of the vitreous chamber in eyes with PS, which is relevant for the relationship between near-work and myopia.⁷⁷ The violet component of sunlight blocked by conventional eyeglasses has been shown to slow myopia progression in preadolescent children wearing violet light-transmitting glasses.⁹⁵ Scleral collagen birefringence has been measured in vivo and found to be related to myopia status and progression, showing promise for clinical monitoring of scleral changes.⁵⁷ ON sheaths traction forces have been suggested to promote PPS,¹³ warranting exploratory studies. Equatorial and anterior eyeball irregularities found in myopic eyes require further investigation.⁴⁷ The traction forces of ON sheaths and oblique muscles could contribute to the occurrence of PS in susceptible individuals (hypothesis formulated in this work), justifying exploratory studies. [Table 3](#) presents an analysis of the studies summarized above.

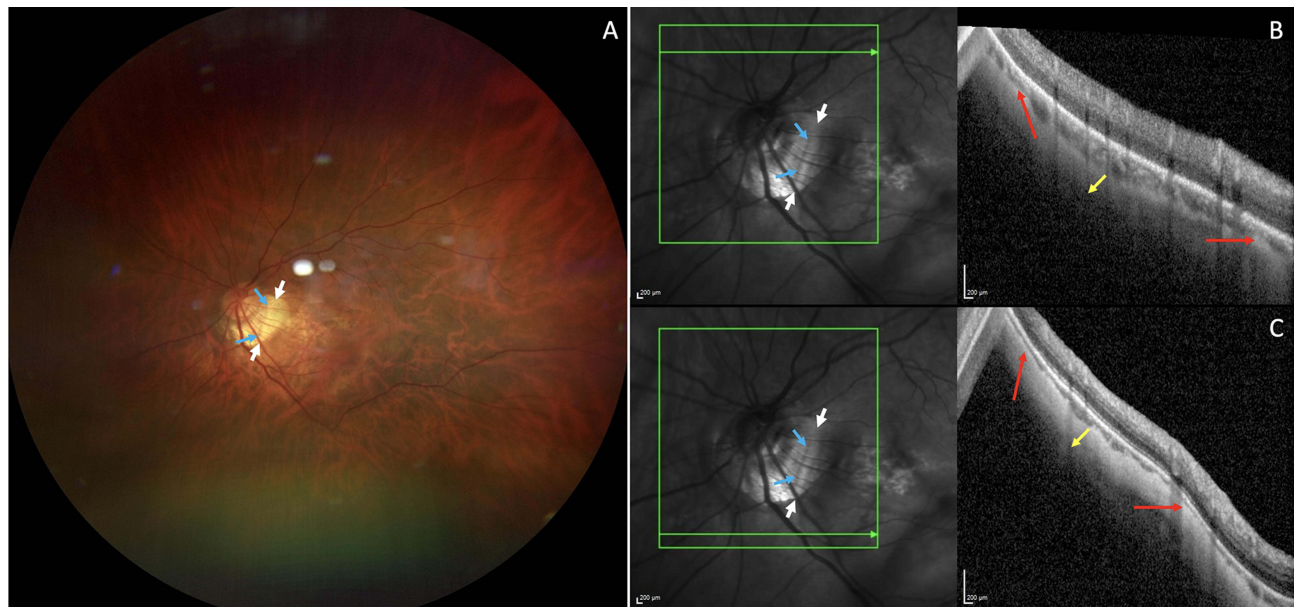


Figure 16 Fundus image of posterior staphyloma (PS) type IX. This PS is the one analyzed in Figures 14 and 15. Axial length: 28.69 mm. **(A)** Widefield fundus image. The signs of PS are slight (relative pallor, subtle edges). **(A–C)** White arrows indicate a discrete ridge best disclosed on infrared images. Blue arrows indicate the arterial circle of Zinn-Haller. **(B and C)** Linear OCT sections as shown in infrared images, located in the upper **(B)** and lower **(C)** peripapillary area. Red arrows indicate a gradual thinning of the choroid toward the edge of the peripapillary component of this compound PS, followed by gradual re-thickening of choroid from the PS edge toward its outward deformation (yellow arrows). The posterior curvature of the eye is sloped temporally. The detailed analysis of the macular component of this PS was presented in Figure 14F.

Genetics and Artificial Intelligence in Myopia Prevention

Recent molecular technologies have identified more than 100 genes and over 20 chromosomal loci associated with myopia.^{96,97} Due to the complex multifactorial determinants of myopia, with numerous phenotypes, its understanding will further benefit from big data for genetic analysis and phenotyping correlation with the collaboration of various research institutes to achieve myopia prevention.^{96,97}

Table 3 Perspectives on Posterior Staphyloma from Some Recent Human Publications

Author Year (Ref)	Clues – Current Data	Hypotheses	Potential Exploration Tracks	Perspectives
Numa 2018 ²¹	Greater curvature irregularities in female, elderly, and eyes with longer axial length documented using SD-OCT	Posterior staphyloma severity can be measured quantitatively through its curvature irregularity	To develop quantitative and standardized methodologies to measure the curvature irregularity of posterior staphyloma	Achieve quantitative standardized methods to assess the severity of posterior staphyloma for randomized studies.
Mori 2021 ⁹⁵	Randomized study shows promise for violet-light glasses to slow myopia progression in pre-adolescent children.	Glasses transmitting violet sunlight slow the progression of myopia	Confirmatory studies	Achieve practical terms of use in combination to outdoor activities
Hoang 2021 ⁷⁷	Gaze down movement increases the vitreous chamber axial volume while other eye gazes do not.	Increase in vitreous chamber axial volume, induced by gaze down movement may be relevant for the role of near and reading activities in myopia.	Confirmatory studies. Exploratory studies to analyze eyeball changes related to eye movements	Analysis of the intraocular and ocular changes during near work and their relationship with myopia development and progression.

(Continued)

Table 3 (Continued).

Author Year (Ref)	Clues – Current Data	Hypotheses	Potential Exploration Tracks	Perspectives
Liu 2022 ⁵⁷	Scleral collagen birefringence is related to myopia status and progression as detected using triple-input polarization-sensitive-OCT technique	In-vivo monitoring of early scleral changes toward pathologic myopia is possible with this technology	Studies for improving this technology	Perform early in-vivo detection of posterior scleral signs indicating pathological changes in myopia
Ehongo 2022 ¹³	Characteristics of peripapillary staphyloma (PPS) analyzed using SD-OCT suggest that PPS is promoted by ON sheaths traction force	ON sheaths traction forces lead to PPS in susceptible individuals	Exploratory studies to confirm the hypothesis. Exploratory studies to find the risk factors to develop PPS.	Achieve an understanding of scleral and ON sheaths factors contributing to PPS and how to counteract them
Nakao 2022 ⁴⁶	Posterior staphyloma deepens more than it enlarges with age. Posterior staphyloma type II depth is related to axial length as documented using UWF-OCT	Posterior staphyloma severity can be measured quantitatively through its depth-to-diameter ratio	To standardize methodologies to measure depth-to-diameter ratio of posterior staphyloma	Achieve quantitative standardized methods to assess the severity of posterior staphyloma for randomized studies
Luo 2023 ⁴⁷	Equatorial and anterior eyeball irregularities documented in myopic subjects using 3D-MRI	Rectus muscles forces might deform the eyeball	Confirmatory studies for the anterior eye-shape irregularities. Exploratory studies for the rectus muscles potential implication.	Achieve an understanding of the scleral and rectus muscles factors favoring the susceptibility for these irregularities
Ehongo 2023 (This article)	Widefield OCT, 3D-MRI, and widefield fundus co-analysis suggests, a correspondence between the edges of the posterior staphyloma and the landmarks of the ON sheaths. It seems the case for oblique muscles, suggesting new insights into the pathogenesis of posterior staphyloma.	ON sheaths and oblique muscles traction forces might lead to posterior staphyloma in susceptible individuals	Exploratory studies to analyze this hypothesis. Exploratory studies to find the determinant factors	Understanding the scleral, ON sheaths and oblique muscles factors favoring the occurrence of posterior staphyloma and how to counteract them

Abbreviations: SD-OCT, spectral domain optical coherence tomography; OCT, optical coherence tomography; ON, optic nerve; PPS, peripapillary staphyloma; UWF, ultra-widefield optical coherence tomography; 3D-MRI, Three-dimensional magnetic resonance imaging.

Many prediction models addressing the onset and progression of myopia in children and teenagers are in development and validation phases.^{98,99}

Wearable devices (smartwatch linked to smartphone) that record time spent outdoors and send feedback to parents and children are in development to encourage children to spend more time outdoors.¹⁰⁰

A cloud-based sensor device attached to the sides of the glasses, objectively and dynamically monitoring the wearer's risky behaviors (near-working distance and its duration)¹⁰¹ is promising. Vibration alert, triggered by risky behavior, has been shown to reduce them in school-aged children.¹⁰¹

Summary

The current and predicted prevalence of myopia are increasing worldwide, and the COVID-19 lockdown has accentuated this trend, making this condition a public health problem more than ever. Its complications, mainly PS are therefore also

expected to increase in the decades to come. The management and prevention of PS that obscures the prognosis of a myopic eye require an understanding of its pathogenesis which remains unknown until now. In particular, why some eyes develop PS and others do not.

In this article, in addition to the already suggested ON sheaths traction forces, I hypothesize that extraocular muscles forces might act on the eyeball, which is summarized as follows.

ON sheaths pull on and distort the eye wall, promoting changes like gamma peripapillary atrophy and complications like PPS and PICC.

The oblique muscles wrap the wall of the eye along their arc of contact and can compress it along this arc during cyclotorsions, which fits with some characteristics of PS. The insertions of the IOM and SOM correspond respectively to the temporal and superior notches of the PS and could witness the pinching of the eyeball by their scleral insertions.

The repetition of these deformations over time would lead to their fixation by remodeling effect, explaining the major influence of age in the prevalence of PS.

The posterior shape of the globe would then reflect a balance between the interaction of ON sheaths, oblique muscles, and biomechanical scleral resistance.

Due to the weakening of ocular structures associated with myopia, the prevalence of PS would be higher in this refractive group.

This hypothesis would explain three indices characterizing PS: the specific pattern underlying the classification of PS, the presence of PS in non-elongated eyes and the transition over time from type II to type IX PS observed in longitudinal studies. Studies are warranted to explore eyeball deformations in relation to eye movements.

Conclusion

Myopia concerns most ophthalmological subspecialties due to its increasing prevalence, early onset, and diversity of complications. Elucidating its pathogenesis and that of its complications, including PS is a key factor for establishing action strategies. It is a multidisciplinary approach, starting with genetics, involving the entire ophthalmological community, and integrating artificial intelligence.

Acknowledgments

The author thanks all the technicians who contributed to acquisition of illustrations recovered for this manuscript.

The author is also grateful to Loïc Blommaert who drew the diagrams of the hypothetic impact of oblique muscles on eyeball deformities.

Funding

No funding was received for this work.

Disclosure

The author reports no conflicts of interest in this work.

References

1. Zhou LX, Shao L, Xu L, Wei WB, Wang YX, You QS. The relationship between scleral staphyloma and choroidal thinning in highly myopic eyes: the Beijing Eye Study. *Sci Rep*. 2017;7(1):9825. PMID: 28852194; PMCID: PMC5575118. doi:10.1038/s41598-017-10660-z
2. Holden BA, Fricke TR, Wilson DA, et al. Global prevalence of myopia and high myopia and temporal trends from 2000 through 2050. *Ophthalmology*. 2016;123(5):1036–1042. PMID: 26875007. doi:10.1016/j.ophtha.2016.01.006
3. Sankaridurg P, Tahhan N, Kandel H, et al. IMI impact of myopia. *Invest Ophthalmol Vis Sci*. 2021;62(5):2. PMID: 33909036; PMCID: PMC8083082. doi:10.1167/iovs.62.5.2
4. Wang J, Li Y, Musch DC, et al. Progression of myopia in school-aged children after COVID-19 home confinement. *JAMA Ophthalmol*. 2021;139(3):293–300. PMID: 33443542; PMCID: PMC7809617. doi:10.1001/jamaophthalmol.2020.6239
5. Ma D, Wei S, Li SM. Progression of myopia in a natural cohort of Chinese children during COVID-19 pandemic. *Graefes Arch Clin Exp Ophthalmol*. 2021;259(9):2813–2820. PMID: 34287693; PMCID: PMC8294263. doi:10.1007/s00417021-05305-x
6. Mohan A, Sen P, Peeush P, Shah C, Jain E. Impact of online classes and home confinement on myopia progression in children during COVID-19 pandemic: digital eye strain among kids (DESK) study 4. *Indian J Ophthalmol*. 2022;70(1):241–245. PMID: 34937246; PMCID: PMC8917570. doi:10.4103/ijo.IJO_1721_21

7. Ma D, Wei S, Li SM, et al. The impact of study-at-home during the COVID-19 pandemic on myopia progression in Chinese children. *Front Public Health*. 2022;9:720514. PMID: 35071149; PMCID: PMC8770940. doi:10.3389/fpubh.2021.720514
8. Ma M, Xiong S, Zhao S, Zheng Z, Sun T, Li C. COVID-19 home quarantine accelerated the progression of myopia in children aged 7 to 12 years in China. *Invest Ophthalmol Vis Sci*. 2021;62(10):37. PMID: 34463719; PMCID: PMC8411864. doi:10.1167/iovs.62.10.37
9. Flitcroft DI, He M, Jonas JB, et al. IMI – defining and classifying myopia: a proposed set of standards for clinical and epidemiologic studies. *Invest Ophthalmol Vis Sci*. 2019;60(3):M20–M30. PMID: 30817826; PMCID: PMC6735818. doi:10.1167/iovs.18-25957
10. Moriyama M, Ohno-Matsui K, Hayashi K, et al. Topographic analyses of shape of eyes with pathologic myopia by high-resolution three-dimensional magnetic resonance imaging. *Ophthalmology*. 2011;118(8):1626–1637. PMID: 21529960. doi:10.1016/j.ophtha.2011.01.018
11. Wang NK, Wu YM, Wang JP, et al. Clinical characteristics of posterior Staphylomas in myopic eyes with axial length shorter than 26.5 millimeters. *Am J Ophthalmol*. 2016;162:180–190.e1. PMID: 26585213. doi:10.1016/j.ajo.2015.11.016
12. Curtin BJ. The posterior staphyloma of pathologic myopia. *Trans Am Ophthalmol Soc*. 1977;75:67–86. PMID: 613534; PMCID: PMC1311542.
13. Ehongo A, Bacq N, Kisma N, et al. Analysis of peripapillary intrachoroidal cavitation and myopic peripapillary distortions in polar regions by optical coherence tomography. *Clin Ophthalmol*. 2022;16:2617–2629. PMID: 35992567; PMCID: PMC9387167. doi:10.2147/OPTH.S376597
14. Wang X, Fisher LK, Milea D, Jonas JB, Girard MJ. Predictions of optic nerve traction forces and peripapillary tissue stresses following horizontal eye movements. *Invest Ophthalmol Vis Sci*. 2017;58(4):2044–2053. PMID: 28384725. doi:10.1167/iovs.16-21319
15. Scarpa A. *Saggio di osservazioni e d'esperienze sulle principali malattie degli occhi [Essay of observations and experiences on the main eye diseases]*. Vol. 10. Pavia: Presso Baldessare Comino; 2015:1801.
16. Spaide RF. Staphyloma: part 1. In: Spaide RF, Ohno-Matsui K, Yannuzzi LA, editors. *Pathologic Myopia*. New York: Springer; 2013:167–176.
17. Ohno-Matsui K. Proposed classification of posterior staphylomas based on analyses of eye shape by three-dimensional magnetic resonance imaging and wide-field fundus imaging. *Ophthalmology*. 2014;121(9):1798–1809. PMID: 24813630. doi:10.1016/j.ophtha.2014.03.035
18. Ohno-Matsui K, Jonas JB. Posterior staphyloma in pathologic myopia. *Prog Retin Eye Res*. 2019;70:99–109. PMID: 30537538. doi:10.1016/j.preteyeres.2018.12.001
19. Shinohara K, Moriyama M, Shimada N, Yoshida T, Ohno-Matsui K. Characteristics of peripapillary Staphylomas associated with high myopia determined by swept-source optical coherence tomography. *Am J Ophthalmol*. 2016;169:138–144. PMID: 27365146. doi:10.1016/j.ajo.2016.06.033
20. Shinohara K, Shimada N, Moriyama M, et al. Posterior Staphylomas in pathologic myopia imaged by widefield optical coherence tomography. *Invest Ophthalmol Vis Sci*. 2017;58(9):3750–3758. PMID: 28738419. doi:10.1167/iovs.17-22319
21. Numa S, Yamashiro K, Wakazono T, et al. Prevalence of posterior staphyloma and factors associated with its shape in the Japanese population. *Sci Rep*. 2018;8(1):4594. PMID: 29545631; PMCID: PMC5854606. doi:10.1038/s41598-018-22759-y
22. Ruiz-Moreno JM, Puertas M, Flores-Moreno I, Almazán-Alonso E, García-Zamora M, Ruiz-Medrano J. Analysis of bilaterality and symmetry of posterior staphyloma in high myopia. *Diagnostics*. 2023;13(16):2680. PMID: 37627937; PMCID: PMC10453303. doi:10.3390/diagnostics13162680
23. Hsiang HW, Ohno-Matsui K, Shimada N, et al. Clinical characteristics of posterior staphyloma in eyes with pathologic myopia. *Am J Ophthalmol*. 2008;146(1):102–110. PMID: 18455142. doi:10.1016/j.ajo.2008.03.010
24. Fledelius HC, Goldschmidt E. Eye shape and peripheral visual field recording in high myopia at approximately 54 years of age, as based on ultrasonography and Goldmann kinetic perimetry. *Acta Ophthalmol*. 2010;88(5):521–526. PMID: 19706012. doi:10.1111/j.1755-3768.2009.01550.x
25. An G, Dai F, Wang R, et al. Association between the types of posterior Staphyloma and their risk factors in pathological myopia. *Transl Vis Sci Technol*. 2021;10(4):5. PMID: 34003983; PMCID: PMC8039568. doi:10.1167/tvst.10.4.5
26. Park HY, Jung Y, Park CK. Posterior staphyloma is related to optic disc morphology and the location of visual field defect in normal tension glaucoma patients with myopia. *Eye*. 2015;29(3):333–341. PMID: 25376120; PMCID: PMC4366452. doi:10.1038/eye.2014.256
27. Flores-Moreno I, Puertas M, Ruiz-Medrano J, Almazán-Alonso E, García-Zamora M, Ruiz-Moreno JM. Influence of posterior staphyloma in myopic maculopathy and visual prognosis. *Eye*. 2023. PMID: 37365301. doi:10.1038/s41433-023-02648-z
28. Gao LQ, Liu W, Liang YB, et al. Prevalence and characteristics of myopic retinopathy in a rural Chinese adult population: the Handan Eye Study. *Arch Ophthalmol*. 2011;129(9):1199–1204. PMID: 21911668. doi:10.1001/archophth.2011.230
29. Guo X, Xiao O, Chen Y, et al. Three-dimensional eye shape, myopic maculopathy, and visual acuity: the Zhongshan Ophthalmic Center-Brien Holden Vision Institute high myopia cohort study. *Ophthalmology*. 2017;124(5):679–687. PMID: 28237427. doi:10.1016/j.ophtha.2017.01.009
30. Henaine-Berra A, Zand-Hadas IM, Fromow-Guerra J, García-Aguirre G. Prevalence of macular anatomic abnormalities in high myopia. *Ophthalmic Surg Lasers Imaging Retina*. 2013;44(2):140–144. PMID: 23438042. doi:10.3928/23258160-20130219-01
31. Frisina R, Baldi A, Cesana BM, Semeraro F, Parolini B. Morphological and clinical characteristics of myopic posterior staphyloma in Caucasians. *Graefes Arch Clin Exp Ophthalmol*. 2016;254(11):2119–2129. PMID: 27106626. doi:10.1007/s00417-016-3359-1
32. Osborne DR, Foulks GN. Computed tomographic analysis of deformity and dimensional changes in the eyeball. *Radiology*. 1984;153(3):669–674. PMID: 6494462. doi:10.1148/radiology.153.3.6494462
33. Swayne LC, Garfinkle WB, Bennett RH. CT of posterior ocular staphyloma in axial myopia. *Neuroradiology*. 1984;26(3):241–243. PMID: 6738856. doi:10.1007/BF00342421
34. Malhotra A, Minja FJ, Crum A, Burrowes D. Ocular anatomy and cross-sectional imaging of the eye. *Semin Ultrasound CT MR*. 2011;32(1):2–13. PMID: 21277487. doi:10.1053/j.sult.2010.10.009
35. Ohno-Matsui K, Akiba M, Modegi T, et al. Association between shape of sclera and myopic retinochoroidal lesions in patients with pathologic myopia. *Invest Ophthalmol Vis Sci*. 2012;53(10):6046–6061. PMID: 22879412. doi:10.1167/iovs.12-10161
36. Tanaka N, Shinohara K, Yokoi T, et al. Posterior staphylomas and scleral curvature in highly myopic children and adolescents investigated by ultra-widefield optical coherence tomography. *PLoS One*. 2019;14(6):e0218107. PMID: 31181108; PMCID: PMC6557512. doi:10.1371/journal.pone.0218107
37. Chang L, Pan CW, Ohno-Matsui K, et al. Myopia-related fundus changes in Singapore adults with high myopia. *Am J Ophthalmol*. 2013;155(6):991–999.e1. PMID: 23499368. doi:10.1016/j.ajo.2013.01.016
38. Ruiz-Moreno JM, Puertas M, Flores-Moreno I, Almazán-Alonso E, García-Zamora M, Ruiz-Medrano J. Posterior Staphyloma as determining factor for myopic maculopathy. *Am J Ophthalmol*. 2023;252:9–16. PMID: 36868340. doi:10.1016/j.ajo.2023.02.017
39. Demer JL. Optic nerve sheath as a novel mechanical load on the globe in ocular ductation. *Invest Ophthalmol Vis Sci*. 2016;57(4):1826–1838. PMID: 27082297; PMCID: PMC4849549. doi:10.1167/iovs.15-18718

40. Lee WJ, Kim YJ, Kim JH, et al. Changes in the optic nerve head induced by horizontal eye movements. *PLoS One*. 2019;14(5):e0216861. Erratum for: *PLoS One*. 201813(9):e0204069. PMID: 31071180; PMCID: PMC6508641. doi:10.1371/journal.pone.0216861
41. Wang X, Chang S, Grinband J, et al. Optic nerve tortuosity and displacements during horizontal eye movements in healthy and highly myopic subjects. *Br J Ophthalmol*. 2022;106(11):1596–1602. PMID: 34039559. doi:10.1136/bjophthalmol-2021-318968
42. Curtin BJ, Iwamoto T, Renaldo DP. Normal and staphylomatous sclera of high myopia. An electron microscopic study. *Arch Ophthalmol*. 1979;97(5):912–915. PMID: 444126. doi:10.1001/archophth.1979.01020010470017
43. Phillips JR, Khalaj M, McBrien NA. Induced myopia associated with increased scleral creep in chick and tree shrew eyes. *Invest Ophthalmol Vis Sci*. 2000;41(8):2028–2034. PMID: 10892839.
44. Jonas JB, Jonas SB, Jonas RA, Holsbach L, Panda-Jonas S. Histology of the parapapillary region in high myopia. *Am J Ophthalmol*. 2011;152(6):1021–1029. doi:10.1016/j.ajo.2011.05.006
45. Jonas JB, Bikbov MM, Wang Y-X, Jonas RA, Panda-Jonas S. Anatomic peculiarities associated with axial elongation of the myopic eye. *J Clin Med*. 2023;12(131):138–140. doi:10.3390/jcm12041317
46. Nakao N, Igarashi-Yokoi T, Takahashi H, Xie S, Shinohara K, Ohno-Matsui K. Quantitative evaluations of posterior Staphylomas in highly myopic eyes by ultra-widefield optical coherence tomography. *Invest Ophthalmol Vis Sci*. 2022;63(8):20. PMID: 35867350; PMCID: PMC9327620. doi:10.1167/iovs.63.8.20
47. Luo N, Wang Y, Alimu S, et al. Assessment of ocular deformation in pathologic myopia using 3-dimensional magnetic resonance imaging. *JAMA Ophthalmol*. 2023:e232869. PMID: 37440241; PMCID: PMC10346513. doi:10.1001/jamaophthalmol.2023.2869
48. McBrien NA, Gentle A. Role of the sclera in the development and pathological complications of myopia. *Prog Retin Eye Res*. 2003;22(3):307–338. PMID: 12852489. doi:10.1016/s1350-9462(02)00063-0
49. Tanaka Y, Shimada N, Ohno-Matsui K. Extreme thinning or loss of inner neural retina along the staphyloma edge in eyes with pathologic myopia. *Am J Ophthalmol*. 2015;159(4):677–682. PMID: 25579643. doi:10.1016/j.ajo.2015.01.004
50. Jonas JB, Ohno-Matsui K, Holbach L, Panda-Jonas S. Histology of myopic posterior scleral staphylomas. *Acta Ophthalmol*. 2020;98(7):e856–e863. Epub 2020 Mar 19. PMID: 32190987. doi:10.1111/aos.14405
51. Rada JA, Nickla DL, Troilo D. Decreased proteoglycan synthesis associated with form deprivation myopia in mature primate eyes. *Invest Ophthalmol Vis Sci*. 2000;41(8):2050–2058. PMID: 10892842.
52. Avetisov ES, Savitskaya NF, Vinetskaya MI, Iomdina EN. A study of biochemical and biomechanical qualities of normal and myopic eye sclera in humans of different age groups. *Metab Pediatr Syst Ophthalmol*. 1983;7(4):183–188. PMID: 6678372.
53. Wang Y, Chen S, Lin J, et al. Vascular changes of the choroid and their correlations with visual acuity in pathological myopia. *Invest Ophthalmol Vis Sci*. 2022;63(12):20. PMID: 36378132; PMCID: PMC9672896. doi:10.1167/iovs.63.12.20
54. Liu Y, Wang L, Xu Y, Pang Z, Mu G. The influence of the choroid on the onset and development of myopia: from perspectives of choroidal thickness and blood flow. *Acta Ophthalmol*. 2021;99(7):730–738. PMID: 33550704. doi:10.1111/aos.14773
55. Nie F, Ouyang J, Tang W, et al. Posterior staphyloma is associated with the microvasculature and microstructure of myopic eyes. *Graefes Arch Clin Exp Ophthalmol*. 2021;259(8):2119–2130. PMID: 33404680; PMCID: PMC8352845. doi:10.1007/s00417-020-05057-0
56. American Academy of Ophthalmology. *Basic and Clinical Science Course 2021–2022, Section 2 Fundamentals and Principles*. American Academy of Ophthalmology; 2022:99.
57. Liu X, Jiang L, Ke M, et al. Posterior scleral birefringence measured by triple-input polarization-sensitive imaging as a biomarker of myopia progression. *Nat Biomed Eng*. 2023;7(8):986–1000. PMID: 37365268; PMCID: PMC10427432. doi:10.1038/s41551-023-01062-w
58. Takano M, Kishi S. Foveal retinoschisis and retinal detachment in severely myopic eyes with posterior staphyloma. *Am J Ophthalmol*. 1999;128(4):472–476. PMID: 10577588. doi:10.1016/s0002-9394(99)00186-5
59. Ohno-Matsui K, Shimada N, Yasuzumi K, et al. Long-term development of significant visual field defects in highly myopic eyes. *Am J Ophthalmol*. 2011;152(2):256–265.e1. PMID: 21664594. doi:10.1016/j.ajo.2011.01.052
60. Ehongo H, Kisma et al. Peripapillary intrachoroidal cavitation at the crossroads of peripapillary myopic changes. *Int J Ophthalmol*. 2023;16(12). doi:10.18240/ijo.2023.12.20
61. Yeh SI, Chang WC, Wu CH, et al. Characteristics of peripapillary choroidal cavitation detected by optical coherence tomography. *Ophthalmology*. 2013;120(3):544–552. PMID: 23207174. doi:10.1016/j.ophtha.2012.08.028
62. Ohno-Matsui K, Shimada N, Akiba M, Moriyama M, Ishibashi T, Tokoro T. Characteristics of intrachoroidal cavitation located temporal to optic disc in highly myopic eyes. *Eye*. 2013;27(5):630–638. PMID: 23470792; PMCID: PMC3650268. doi:10.1038/eye.2013.16
63. Okuma S, Mizoue S, Ohashi Y. Visual field defects and changes in macular retinal ganglion cell complex thickness in eyes with intrachoroidal cavitation are similar to those in early glaucoma. *Clin Ophthalmol*. 2016;10:1217–1222. PMID: 27418805; PMCID: PMC4935007. doi:10.2147/OPHTH.S102130
64. Ehongo A, Dugauquier A, Kisma N, et al. Myopic (Peri)papillary changes and visual field defects. *Clin Ophthalmol*. 2023;17:3295–3306. doi:10.2147/OPHTH.S404167
65. Fujimoto S, Miki A, Maruyama K, et al. Three-dimensional volume calculation of intrachoroidal cavitation using deep-learning-based noise reduction of optical coherence tomography. *Transl Vis Sci Technol*. 2022;11(7):1. PMID: 35802370; PMCID: PMC9279919. doi:10.1167/tvst.11.7.1
66. Jonas JB, Ohno-Matsui K, Holbach L, Panda-Jonas S. Association between axial length and horizontal and vertical globe diameters. *Graefes Arch Clin Exp Ophthalmol*. 2017;255(2):237–242. PMID: 27473372. doi:10.1007/s00417-016-3439-2
67. Jonas JB, Ohno-Matsui K, Jiang WJ, Panda-Jonas S. Bruch membrane and the mechanism of myopization: a new theory. *Retina*. 2017;37(8):1428–1440. doi:10.1097/IAE.0000000000001464
68. Spaide RF, Akiba M, Ohno-Matsui K. Evaluation of peripapillary intrachoroidal cavitation with swept source and enhanced depth imaging optical coherence tomography. *Retina*. 2012;32(6):1037–1044. PMID: 22466483. doi:10.1097/IAE.0b013e318242b9c0
69. Chang MY, Shin A, Park J, et al. Deformation of optic nerve head and peripapillary tissues by horizontal duction. *Am J Ophthalmol*. 2017;174:85–94. PMID: 27751810; PMCID: PMC5812679. doi:10.1016/j.ajo.2016.10.001
70. Wang X, Teoh CKG, Chan ASY, et al. Biomechanical properties of Bruch's membrane-choroid complex and their influence on optic nerve head biomechanics. *Invest Ophthalmol Vis Sci*. 2018;59(7):2808–2817. PMID: 30029276. doi:10.1167/iovs.17-22069

71. Abdelhady A, Patel BC, Aslam S, Al Aboud DM. Anatomy, head and neck: eye superior oblique muscle. In: *StatPearls*. Treasure Island (FL): StatPearls Publishing; 2023. PMID: 30725837.
72. Shumway CL, Motlagh M, Wade M. Anatomy, head and neck, eye extraocular muscles. In: *StatPearls*. Treasure Island (FL): StatPearls Publishing; 2023. PMID: 30137849.
73. Kumar V, Murlimanju BV, Devika P, et al. An anatomical study of the inferior oblique muscle with emphasis on its nerve entry. *Chang Gung Med J*. 2011;34(3):293–297. PMID: 21733359.
74. Gupta N, Patel BC. Anatomy, head and neck: eye inferior oblique muscles. In: *StatPearls*. Treasure Island (FL): StatPearls Publishing; 2023. PMID: 31424837.
75. American Academy of Ophthalmology. *Basic and Clinical Science Course™2021–2022, Section 6_Pediatric Ophthalmology and Strabismus*. 2022:21–32.
76. Ellabban AA, Tsujikawa A, Matsumoto A, et al. Three-dimensional tomographic features of dome-shaped macula by swept-source optical coherence tomography. *Am J Ophthalmol*. 2013;155(2):320–328.e2. PMID: 23127750. doi:10.1016/j.ajo.2012.08.007
77. Hoang QV, Chang S, Yu DJG, Yannuzzi LA, Freund KB, Grinband J. 3-D assessment of gaze-induced eye shape deformations and downgaze-induced vitreous chamber volume increase in highly myopic eyes with staphyloma. *Br J Ophthalmol*. 2021;105(8):1149–1154. PMID: 32830122. doi:10.1136/bjophthalmol-2020-316084
78. He MG, Xiang F, Zeng YF, et al. Effect of time spent outdoors at school on the development of myopia among children in China: a randomized clinical trial. *JAMA*. 2015;314(11):1142–1148. doi:10.1001/jama.2015.10803
79. Wu PC, Chen CT, Lin KK, et al. Myopia prevention and outdoor light intensity in a school-based cluster randomized trial. *Ophthalmology*. 2018;125(8):1239–1250. doi:10.1016/j.ophtha.2017.12.011
80. Wu PC, Chuang MN, Choi J, et al. Update in myopia and treatment strategy of atropine use in myopia control. *Eye*. 2019;33(1):3–13. PMID: 29891900; PMCID: PMC6328548. doi:10.1038/s41433-018-0139-7
81. Yam JC, Jiang Y, Tang SM, et al. Low-concentration atropine for myopia progression (LAMP) study: a randomized, double-blinded, placebo-controlled trial of 0.05%, 0.025%, and 0.01% atropine eye drops in myopia control. *Ophthalmology*. 2019;126(1):113–124. doi:10.1016/j.ophtha.2018.05.029
82. Huang J, Wen D, Wang Q, et al. Efficacy comparison of 16 interventions for myopia control in children: a network meta-analysis. *Ophthalmology*. 2016;123(4):697–708. doi:10.1016/j.ophtha.2015.11.010
83. Bullimore MA, Ritchey ER, Shah S, Leveziel N, Bourne RRA, Flitcroft DI. The risks and benefits of myopia control. *Ophthalmology*. 2021;128(11):1561–1579. PMID: 33961969. doi:10.1016/j.ophtha.2021.04.032
84. Kinoshita N, Konno Y, Hamada N, Kanda Y, Shimmura-Tomita M, Kakehashi A. Additive effects of orthokeratology and atropine 0.01% ophthalmic solution in slowing axial elongation in children with myopia: first year results. *Jpn J Ophthalmol*. 2018;62(5):544–553. doi:10.1007/s10384-018-0608-3
85. Kinoshita N, Konno Y, Hamada N, et al. Efficacy of combined orthokeratology and 0.01% atropine solution for slowing axial elongation in children with myopia: a 2-year randomized trial. *Sci Rep*. 2020;10:544–553. doi:10.1038/s41598-020-69710-8
86. Chen YX, Liao CM, Tan Z, He MG. Who needs myopia control? *Int J Ophthalmol*. 2021;14(9):1297–1301. PMID: 34540602; PMCID: PMC8403852. doi:10.18240/ijo.2021.09.01
87. Cooper J, Aller T, Smith EL 3rd, Chan K, Dillehay SM, O'Connor B. Retrospective analysis of a clinical algorithm for managing childhood myopia progression. *Optom Vis Sci*. 2023;100(1):117–124. PMID: 36542468. doi:10.1097/OPX.0000000000001978
88. Wildsoet CF, Chia A, Cho P, et al. IMI – interventions for controlling myopia onset and progression report. *Invest Ophthalmol Vis Sci*. 2019;60(3):M106–M131. Erratum in: *Invest Ophthalmol Vis Sci*. 2019 Apr 1;60(5):1768. PMID: 30817829. doi:10.1167/iovs.18-25958
89. Németh J, Tapasztó B, Aclimandos WA, et al. Update and guidance on management of myopia. European society of ophthalmology in cooperation with international myopia institute. *Eur J Ophthalmol*. 2021;31(3):853–883. Epub 2021 Mar 5. PMID: 33673740; PMCID: PMC8369912. doi:10.1177/1120672121998960
90. Huang W, Duan A, Qi Y. Posterior scleral reinforcement to prevent progression of high myopia. *Asia Pac J Ophthalmol*. 2019;8(5):366–370. PMID: 31513040; PMCID: PMC6784774. doi:10.1097/APO.0000000000000257
91. Gawargious BA, Le A, Lesgart M, Ugradar S, Demer JL. Differential regional stiffening of sclera by collagen cross-linking. *Curr Eye Res*. 2020;45(6):718–725. PMID: 31735063; PMCID: PMC7239705. doi:10.1080/02713683.2019.1694157
92. Blackburn BJ, Rollins AM, Dupps WJ Jr. Biomechanics of ophthalmic crosslinking. *Transl Vis Sci Technol*. 2021;10(5):8. PMID: 34328498; PMCID: PMC8327749. doi:10.1167/tvst.10.5.8
93. Wang M, Corpuz CCC, Zhang F. Shaping eyeballs by scleral collagen cross-linking: a hypothesis for myopia treatment. *Front Med*. 2021;8:655822. PMID: 34277654; PMCID: PMC8282923. doi:10.3389/fmed.2021.655822
94. Shinohara K, Yoshida T, Liu H, et al. Establishment of novel therapy to reduce progression of myopia in rats with experimental myopia by fibroblast transplantation on sclera. *J Tissue Eng Regen Med*. 2018;12(1):e451–e461. PMID: 28401697. doi:10.1002/term.2275
95. Mori K, Torii H, Hara Y, et al. Effect of Violet light-transmitting eyeglasses on axial elongation in myopic children: a randomized controlled trial. *J Clin Med*. 2021;10(22):5462. PMID: 34830743; PMCID: PMC8624215. doi:10.3390/jcm10225462
96. Cai XB, Shen SR, Chen DF, Zhang Q, Jin ZB. An overview of myopia genetics. *Exp Eye Res*. 2019;188:107778. PMID: 31472110. doi:10.1016/j.exer.2019.107778
97. Zhang C, Zhao J, Zhu Z, et al. Applications of artificial intelligence in myopia: current and future directions. *Front Med*. 2022;9:840498. PMID: 35360739; PMCID: PMC8962670. doi:10.3389/fmed.2022.840498
98. Lin H, Long E, Ding X, et al. Prediction of myopia development among Chinese school-aged children using refraction data from electronic medical records: a retrospective, multicentre machine learning study. *PLoS Med*. 2018;15:e1002674. doi:10.1371/journal.pmed.1002674
99. Yang X, Chen G, Qian Y, et al. Prediction of myopia in adolescents through machine learning methods. *Int J Environ Res Public Health*. 2020;17:463. doi:10.3390/ijerph17020463
100. Verkicharla PK, Ramamurthy D, Nguyen QD, et al. Development of the FitSight fitness tracker to increase time outdoors to prevent myopia. *Transl Vis Sci Technol*. 2017;6(3):20. PMID: 28660095; PMCID: PMC5477631. doi:10.1167/tvst.6.3.20
101. Cao Y, Lan W, Wen L, et al. An effectiveness study of a wearable device (Clouclip) intervention in unhealthy visual behaviors among school-age children: a pilot study. *Medicine*. 2020;99:e17992. doi:10.1097/md.00000000000017992

Clinical Ophthalmology

Dovepress

Publish your work in this journal

Clinical Ophthalmology is an international, peer-reviewed journal covering all subspecialties within ophthalmology. Key topics include: Optometry; Visual science; Pharmacology and drug therapy in eye diseases; Basic Sciences; Primary and Secondary eye care; Patient Safety and Quality of Care Improvements. This journal is indexed on PubMed Central and CAS, and is the official journal of The Society of Clinical Ophthalmology (SCO). The manuscript management system is completely online and includes a very quick and fair peer-review system, which is all easy to use. Visit <http://www.dovepress.com/testimonials.php> to read real quotes from published authors.

Submit your manuscript here: <https://www.dovepress.com/clinical-ophthalmology-journal>